Dynamic methods in plasma physics

V. E. Fortov

Institute of Chemical Physics, Academy of Sciences of the USSR
Usp. Fiz. Nauk **138**, 361–412 (November 1982)

Hydrodynamic methods of generating and diagnosing dense plasmas with strong interparticle interaction are reviewed. Experiments in shock and isentropic compression of matter to produce Boltzmann and degenerate plasma with maximum pressures in the tens of megabars are discussed. A method for isentropic expansion of metals that have been compressed by strong shock waves, which makes it possible to investigate a broad range of the phase diagram, including the high-temperature boiling curve and the neighborhood of the critical point, is described. The experimental schemes and designs of compressed-air and explosion-type nonideal-plasma generators and the diagnostic tools used are discussed. The results of experiments with nonideal plasmas are reported, and the influence of the interparticle interaction on the thermodynamic, electrophysical, and optical properties of the strongly compressed plasma is analyzed on the basis of theoretical models. The properties of ultrahigh-pressure plasmas and prospects for laser electrodynamic and electroexplosive methods of generating strong shock waves in condensed media are discussed.

PACS numbers: 52.50.Lp, 52.25.Kn, 52.25.Lp, 52.20. – j

TABLE OF CONTENTS

1. INTRODUCTION

The behavior of plasma, the state of matter most commonly encountered in nature, under conditions of strong interparticle interaction has always interested investigators because of the wide variety and uncommon nature of its physical properties. Nonideal plasma is formed and determines the physical properties of matter in a broad region of the phase diagram extending from the solid and liquid states all the way to the neutral gas, and including the boiling and melting phase boundaries and the region of the "metal-dielectric" transition in disordered systems.[1,2]

Recently, purely pragmatic interest in the study of high-pressure plasma has also increased in connection with work on a number of crucial energy projects and devices whose action is based on pulsed local concentration of energy in dense media. The nonideal plasma is a promising working fluid in powerful MHD generators, power-generating stations,[3] rocket engines[4] with gaseous-phase reactors, and in industrial plasma-chemical installations.[5] Nonideal plasmas are formed in nuclear explosions,[6] on explosive vaporization of pinch and magnetocumulative generator liners,[7] and when strong shock waves, laser radiation, and electron beams act on condensed matter,[8] as well as in many other cases. In studying the heavy giant planets of the solar system, investigators must also deal with nonideal plasmas formed during hypersonic motion of space vehicles in their dense atmospheres.[9] Knowledge of the physical characteristics of the dense plasma is especially necessary in work leading to pulsed thermonuclear fusion, which can be brought about by laser, electron, ion, or explosive compression of spherical targets.[10,239]

These circumstances provide a strong and abiding stimulus to the theoretical and experimental work begun during the last decade on the influence of nonideality on plasma physical properties.

A considerable number of reviews and monographs has been devoted to theoretical methods of description of the nonideal plasma (see, for example, Refs. 1, 2, 5, 11–16, 195, and 204). The physical properties of plasma are radically simplified at extremely high pressures and temperatures, at which the kinetic energy is considerably greater than the energy of the interparticle interaction and homogeneous-degeneration or Boltzmann-ideal-gas models are fully valid. The weak interparticle interaction can then be taken into account by perturba-

 0038-5670/82/110781-29$01.80

tion-theory methods within the framework of the classical (Debye-Hueckel theory) or quasiclassical (Thomas-Fermi theory) approximations to the self-consistent-field method. In the nonideal plasma, the interaction energy is comparable to or exceeds the kinetic energy of particle motion, making it impossible to use the perturbation-theory apparatus[12] for such systems and difficult to make a properly conditioned choice of the pseudopotential of the electron-ion interaction when nonparametric Monte-Carlo methods are used.[14] Adequate kinetic equations have not yet been formulated for the strongly interacting plasma, since it has not been possible here to separate the characteristic elementary process times without ambiguity and the temporal evolution of the system under the action of the external field may possibly be no longer described by a Markoff process.[15] To analyze the physical properties of the nonideal plasma, it is therefore necessary to use highly qualitative, heuristic models[1,2] based on extrapolations of notions obtained for the rarefied plasma as to the role of collective and quantum effects in the case of Coulomb interaction—models that predict the appearance of fundamentally new physical effects such as metallization[12,13] and clusterization[16,194] of the plasma and formation of previously unknown exotic plasma phases.[1,2,5] It is natural that experimental verification of these predictions should be one of the most urgent and intriguing problems of contemporary plasma physics.

The basic difficulty in generating nonideal plasma states arises from the need for high local energy concentrations in dense media. The pressures and temperatures developed are generally much higher than the hot-strength limits of the structural materials used in the devices, and this makes it necessary to conduct experiments in a forced pulsed regime at a high power level. Further difficulties in studying nonideal plasma are caused by the nearly complete lack of developed diagnostic methods owing to the optical opacity of these plasmas and the arbitrariness with which electrons are defined as free and bound.

It has become possible only very recently to make varying degrees of progress in overcoming these difficulties. Two sharply defined directions have emerged: electrical and dynamic methods for generation of nonideal plasma. In the former, which has become the classical trend in plasma physics, the plasma forms as a result of Joule heating of matter through which electric-current pulses are passed, and the plasma is confined by massive solid capillary walls or a high-pressure gas. The progress made in this direction has been analyzed in detail in recent reviews.[17-19]

The dynamic alternatives to the electrical methods are based on accumulation of energy in the matter under study either as a result of viscous dissipation in the fronts of shock waves, which compress and accelerate the matter and heat it irreversibly, or as a result of an adiabatic change in the pressure of the medium. Without going into a detailed comparison of the electrical and dynamic techniques, we note that the high purity and homogeneity of the test volume, the absence of electric and magnetic fields, which make diagnosis difficult and cause development of various instabilities in the plasma, the high reproducibility of the results, and the possibility of obtaining extremely high parameters make the dynamic methods a convenient way to obtain and investigate the physical properties of strongly nonideal media under extreme conditions. Moreover, application of the general laws of mass, momentum, and energy conservation reduces (Sec. 2) the recording of thermodynamic characteristics of the plasma to determining the kinematic parameters of the motion of the shock and contact discontinuities—an additional significant advantage of the dynamic methods.

The use of shock waves in high-pressure physics has made it possible to produce condensed-matter pressures in the hundreds of thousands and millions of atmospheres under controlled conditions and to conduct broad thermodynamic, optical, and electrophysical[20-24] studies under those conditions. Use of these methods in nonideal-plasma physics had made it possible to advance significantly up the scale of plasma pressures and temperatures and to make laboratory studies of states with extremely high energy concentrations. For example, physical measurements have been made in the part of the phase diagram that is inaccessible to traditional plasma-experimentation methods.

The present review represents an attempt at a critical organization of recent results from experimental dynamic-method studies of the nonideal plasma. We shall discuss two methods for dynamic production of nonideal plasmas—the shock method and adiabatic compression (Secs. 3, 4, 8) and adiabatic expansion (Sec. 6) of shock-compressed matter.

Shock compression is most effective for studying nondegenerate plasmas of substances that are gases in the initial state. A combination of heated compressed-air, electric-discharge, and explosion-type shock tubes has yielded information on the thermodynamic, electrophysical and optical properties of plasma at pressures up to 110 kbar, electron concentrations of $\sim 10^{23}$ cm^{-3} and densities up to 4.5 g/cm^3, which are 1.5 times higher than the crystallographic density of xenon. Under such conditions, the Coulomb interaction energy is an order of magnitude larger than the kinetic energy of particle motion, so that from the physical standpoint the plasma resembles a liquid, from which it differs in its more complex interparticle-interaction spectrum. The behavior of plasma at ultramegabar pressures is now attracting increased interest from the standpoint of clarifying the role of shell effects and establishing the lower limit of validity of the quasiclassical equation-of-state models. Nuclear explosions[6,177], lasers, and rapid electrical explosion of metal foils are now being used to reach this range of pressures (Sec. 8).

Shock and isentropic compression techniques make it possible to produce high pressures and temperatures in media of increased density, but thermodynamic limitations make it impossible to investigate the boiling curve and the near-critical state of metals. Isentropic expansion of metals (Sec. 6) that have first been com-

pressed in the fronts of strong shock waves is an effective way of obtaining plasmas with subsolid densities. This technique makes it possible to investigate a broad range of the metal phase diagram, extending from the strongly compressed metallic liquid all the way to the ideal gas and including the region of the nonideal degenerate and Boltzmann plasma and the neighborhood of the critical point.

Recording of decompression isentropes has provided a basis for construction of broad-range equations of state and has made it possible to draw more definite interferences as to the qualitative form of the phase diagram of matter at high pressures and temperatures. This question is not trivial for the strongly nonideal plasma in light of the numerous predictions[2, 5, 12, 13, 189, 197] of exotic phase transitions governed by the "metal-to-dielectric" transformation and by the strong interactions of charged particles with one another and with neutral particles. We shall briefly discuss related experimental studies in Sec. 7.

2. PRINCIPLES OF DYNAMIC PLASMA GENERATION AND DIAGNOSTICS

In a plasma with developed ionization, the interaction between charged particles is dominant compared to the other forms of nonideality—"charge-neutral" and "neutral-neutral"—and is characterized by the ratio $\Gamma = \varepsilon_e/\varepsilon_k$ of the average Coulomb interaction energy $\varepsilon_e = ze^2/\rho_e$ (ρ_e is the screening radius) to the particle kinetic energy ε_k. The degeneracy of the plasma is determined by the parameter $\eta_e\lambda^3$, where $\lambda = \sqrt{\hbar^2/2\pi mkT}$ is the thermal deBroglie wavelength. In a rarefied high-temperature plasma (Fig. 1), the Coulomb interaction is small, $\Gamma \ll 1$, and its contribution can be calculated from perturbation theory in the form of corrections[12] to the model of the ideal Boltzmann gas ($\eta_e\lambda^3 \ll 1$)—the "Debye" region in Fig. 1. Isothermal compression of such a plasma at $T < Ry = e^4m/2\hbar^2 = 150\,000$ K results in an increase in the Coulomb interaction energy, which, after crossing the line $\Gamma = 1$, exceeds the kinetic energy of particle motion. This makes it difficult to describe the nonideal plasma theoretically and impossible to apply perturbation theory, forcing us to use qualitative physical models. Further compression of the plasma increases the nonideality, but only up to a certain limit. This is because electron degeneration occurs at the boundary $n\lambda^3 = 1$ as the density increases; the kinetic energy scale is the Fermi energy $\varepsilon_F = \hbar^2 n_e^{2/3}/2m_e$, which increases with increasing density of the plasma. Therefore the degenerate electron plasma becomes increasingly ideal as it is compressed, and above the boundary $\varepsilon_F \sim e^2 n_e^{1/3}$ it can be described with a quasihomogeneous Fermi electron gas model with allowance for interaction effects either within the framework of the asymptotic theories[2,12] or in accordance with the Thomas-Fermi cell model,[11] which takes into account the presence of positively charged nuclei. Therefore only states with extremely high pressures and temperatures, states situated on the periphery of the phase diagram, are accessible to consistent theoretical analysis. We see that the region of existence of the nonideal plasma is bounded and situated in Fig. 1 within the triangle formed by $\varepsilon_F \sim e^2 n^{1/3}$ and $\Gamma \sim 1$, the upper part of which pertains to the degenerate plasma, while its lower part pertains to the Boltzmann plasma,[1)] and the highest attainable values of the nonideality parameter are finite and no larger than a few units.

On the real PV phase diagram, the nonideal plasma occupies an extremely broad region (Fig. 2) directly contiguous to and, in fact, intruding into[12] the region of the condensed state, where quantitative description is difficult because it is determined by the specific electron spectra of the atoms and molecules. Therefore

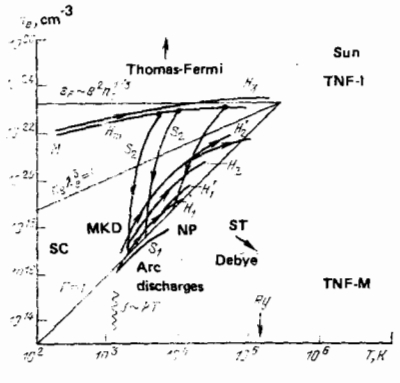

FIG. 1. Existence regions of nonideal plasma. M—metals, SC—semiconductors, MHD—magnetohydrodynamic generators, NP—plasma-reactor nuclear powerplants, ST—shock tubes, TNF-I, TNF-M—controlled thermonuclear fusion installations with inertial and magnetic confinement. The wavy line indicates the beginning of ionization; the arrows indicate the direction of decreasing interparticle interaction and simplification of physical description of the plasma properties. Experiment: H_1, H'_1—compression of cesium plasma by direct and reflected shock waves, S_1—adiabatic compression of cesium (Sec. 3); H_2, H'_2—compression of inert gases by direct and reflected shock waves (Sec. 4); H_3—compression of solid and H_m of porous metals by shock waves (Sec. 8), S_2—adiabatic expansion of shock-compressed metals (Sec. 6).

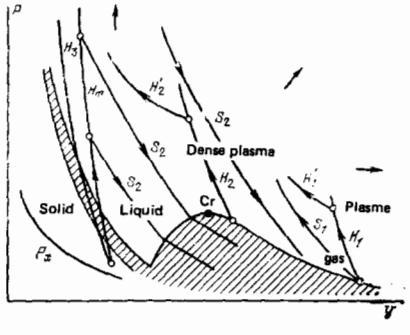

FIG. 2. Diagram explaining principles of dynamic plasma generation. P_x—limit of compressibility of matter—"cold" ($T = 0$) compression curve. Two-phase regions during melting and vaporization are shaded. Cr is the critical point. The circles are the initial states of the medium. Remaining notation as in Fig. 1.

1) The Coulomb interaction is small also at temperatures below the ionization potential, $T < J$, owing to the weak thermal ionization of the plasma, with the result that conditions for generation of a Boltzmann plasma by overheating are optimized (see Fig. 6).

priority should be given here to experimental, and primarily dynamic,[20-24] methods, which permitted elegant earlier measurement of the thermodynamic, optical, and electrophysical properties of condensed matter at megabar pressures. Modern high-temperature experimental techniques have made it possible to move forward into the region of the boiling curve and the vicinity of the critical points of the low-boiling metals Hg, Cs, and Rb[17,18] and to investigate the liquid-phase region at $P \leq 4$ kbar and $T \leq 5 \cdot 10^3$ K.[25] But for the overwhelming majority of the other metals (which account for about 80% of all elements of the periodic system), not only have critical parameters not yet been found, but even the qualitative form of the phase diagram has not been established, since most of it is occupied by the nonideal-plasma region, which is inaccessible to traditional experimental techniques.

To produce a plasma with strong interparticle interaction, it is necessary to ensure significant energy release in a medium of elevated density. Generally, the pressures and temperatures that are developed are quite far above the hot-strength limits of the structural materials used in the installations, so that it is possible to preserve the plasma only for the short time determined by its inertial dispersal. This makes it necessary to conduct the experiment in a forced pulsed regime at a high power level, and the corresponding experimental arrangements must ensure rapid supply of energy to the object under study, which must be large enough to permit reliable diagnosis. Existing possibilities for plasma generation are presented in Table I, which gives characteristic (not necessarily maximum) parameters for the energy sources used to compress and heat the matter. Here, because of the limitations on degeneracy and overheating of plasma that were cited in Sec. 1, the extreme-value parameters in Table I do not correspond at all to the strongest Coulomb-nonideality effects.

TABLE I. Energy sources and experimental arrangements used in the physics of high energy concentrations: 1) primary

primary energy source	final form	energy density, MJ/cm³	temperature, eV	pressure, bar	total energy, MJ	duration, sec	power, W
chemical explosives		10^{-2}	0.5	$5 \cdot 10^5$	10^2	10^{-7}	10^{10} (per cm²)
	metal plates	0.8	6.0	10^7	3	10^{-6}	10^{12}
	1-MOe magnetic field	$4 \cdot 10^{-3}$	0.3	$5 \cdot 10^4$	5	10^{-6}	$5 \cdot 10^{12}$
	25-MOe magnetic field	2.5	200	$2.5 \cdot 10^7$	1	10^{-7}	10^{13}
	explosion-type plasma generators	10^{-2}	60	10^5	30	10^{-6}	10^{12}
nuclear explosives		10^4	10^7	10^{10}	10^{11}	10^{-9}	10^{22}
	neutron heating	10	50	$2 \cdot 10^7$	10^9	10^{-8}	10^{15}
	shock waves in solid	5	50	$5 \cdot 10^7$	10^4	$3 \cdot 10^{-6}$	10^{15}
	shock waves in gas	0.3	40	$2 \cdot 10^5$	10^7	10^{-5}	10^{18}
compressed gas	adiabatic compression	$2 \cdot 10^{-5}$	0.3	150	10^3	$6 \cdot 10^{-3}$	10^5
	compressed-air shock tubes	10^{-4}	1	250	10^{-2}	10^{-4}	$3 \cdot 10^8$
	combustion shock tubes	10^{-6}	2	10	$2 \cdot 10^{-2}$	$3 \cdot 10^{-1}$	10^8
	shock tubes, electrical discharge	10^{-7}	2	1	10^{-2}	10^{-1}	10^8
capacitor		10^{-7}	—	—	40	10^{-5}	10^{12}
rotary machine		10^{-3}	—	—	500	10^{-1}	10^{12}
induction accumulator		10^{-4}	—	—	200	10^{-1}	10^{12}
accumulator		$5 \cdot 10^{-4}$	—	—	1000	10^{-3}	10^{12}
	rapid explosion of wires	$5 \cdot 10^{-2}$	4	10^5	10^{-3}	10^{-6}	10^9
	slow explosion of wires	$2 \cdot 10^{-2}$	0.5	$5 \cdot 10^2$	10^{-3}	10^{-4}	10^7
	pulse discharges	10^{-3}	10	10^4	10^{-4}	10^{-3}	10^9
	plasma focus	10^{-2}	1000	10	10^{-4}	10^{-5}	10^{10}
	high-pressure arcs	10^{-5}	2	10^4	10^{-4}	steady	10^4
	furnace experiments	10^{-3}	0.3	$5 \cdot 10^3$	10^{-3}	steady	10^3
laser		10^{-6}	—	—	$0.5 \cdot 10^{-3}$	10^{-10}	10^{13}
	target	10^4	$5 \cdot 10^4$	10^8	0.5	10^{-10}	10^{22}
electron beam		10^{-6}	—	—	1	10^{-8}	10^{13}
	target	510	$5 \cdot 10^3$	10^7	0.1	10^{-8}	10^{13}

Dynamic generation methods are based on hydrodynamic heating of matter as a result of viscous energy dissipation in shock-wave fronts or of adiabatic compression of the medium.[26] The three techniques that are now most widely used in plasma research are isentropic and shock compression and isentropic expansion of matter that has first been compressed by a shock wave. The use of various energy sources to generate the shock waves and compression waves—compressed gas and gas that has been heated by an electric discharge, chemical[20] and nuclear explosives,[6] and strong laser and neutron fluxes[6,219]—has made it possible to produce nonideal plasmas in a broad range of densities from solid to gaseous, at record-high pressures in the tens of millions of atmospheres and with maximum temperatures in the tens of electron-volts.

Many of these data have been obtained with shock waves that compress and irreversibly heat solid or gaseous matter. The latter case is especially convenient for production of the strongly nonideal Boltzmann plasma (Secs. 3–5), which is formed on shock compression of high-pressure gases the initial states of which are (see Fig. 2) in the neighborhood of the saturation curve (cesium, argon) or even at supercritical conditions (xenon). It is possible, by recording a state of single H- and double H′ compression, to obtain a plasma of supercritical parameters at pressures P up to 110 kbar and temperatures T up to 10^5 K and to penetrate into the region of the condensed state from the "gaseous-phase" side. Adiabatic compression of saturated cesium vapor (S_1; see Fig. 2) makes it possible (Sec. 3) to attain a lower degree of plasma heating at which the interaction of charges with neutral particles dominates. Compression of metals by strong shock waves[20-24] formed on detonation of condensed explosives brings the metal to a state with pressure up to 5–10 mbar and temperatures in the tens of thousands of degrees, in which the metal is fused and the essential result is a disorganized electron-ion plasma in which the electron component is degenerate or partially degenerate.

The use of powerful explosions,[27-32] neutron radiation formed on detonation of nuclear devices,[6] and concentrated laser radiation[171-173,219] raises the pressure to tens and hundreds of megabars, forming a basis for extrapolation testing of quasiclassical theories.[11,31]

It is a distinctive property of the shock-wave techniques that they produce high pressures and temperatures in compressed media, while the region of low plasma densities (including the boiling curve and the neighborhood of the critical point) is inaccessible to them. The plasma state intermediate between solid and gas can be investigated by the isentropic-expansion technique (Sec. 6), which is based on generation of plasma in the adiabatic expansion of condensed matter (S_2; see Fig. 2) that has been compressed and irreversibly heated in the front of a strong shock wave. This technique has made it possible to investigate the properties of metals in a broad region of the phase diagram from the strongly compressed condensed state all the way to the ideal gas, including the region of the degenerate and Boltzmann low-temperature plasma, near-critical and two-phase states, and the region of the "metal-dielectric" transition.

Dynamic diagnostic methods are based[20] on use of the relation between the thermodynamic properties of the medium being studied and the hydrodynamic phenomena observed in experiment.[26] This relation is expressed in general form by a system of nonlinear (three-dimensional in the space coordinate) differential equations of nonstationary gasdynamics, complete solution of which is beyond the capabilities of even the most powerful modern computers.[2)] For this reason, an effort is made in dynamic studies to use[20,26] self-preserving solutions such as the stationary shock wave and the centralized Riemann rarefaction wave, which express the conservation laws in simple algebraic or integral form. To use these simple solutions in experiments, it is necessary to ensure the self-preserving property of the corresponding flow regimes.

When a stationary shock wave propagates through matter, the mass, momentum, and energy conservation laws[26]

$$\frac{V}{V_0}=\frac{D-u}{D}, \quad P=P_0-\frac{Du}{V_0}, \qquad E-E_0=\frac{1}{2}(P+P_0)(V_0-V), \tag{2.1}$$

are satisfied on the wave front and enable us to find the hydrodynamic and thermodynamic characteristics of the matter from records of any two of the five parameters P, E, V, D, and u that characterize the shock front. The velocity D of the shock wave can be registered most easily and accurately by baseline methods. The choice of the second measured parameter depends on the specific conditions of the experiment.

Analysis of the errors in the quantities entering into (2.1) indicates[33] that it is advisable for strongly compressible ("gaseous") media to register the density $\rho=v^{-1}$ of the shock-compressed matter. A technique for making these measurements on the basis of measurements of the absorption of "soft" x-rays by cesium (Sec. 3), argon (Sec. 4), and air (Sec. 7) plasmas has now been developed. At lower system compressibilities (for condensed media), acceptable accuracy is ensured[20] by recording the mass velocity u. It has been possible in this way to find states of degenerate metal plasmas[20] and dense Boltzmann argon and xenon plasmas (Sec. 4). The pressure and density are measured in adiabatic-compression experiments,[34-35] which, with the adiabaticity condition, corresponds to

$$E=\int_{V_0}^{V} P\,dV.$$

In experiments to record isentropic-expansion curves of shock-compressed matter (Sec. 6), states in the centralized unloading wave are described by Riemann integrals[26]:

$$V=V_H+\int_{P}^{P_H}\left(\frac{du}{dP}\right)^2 dP, \quad E=E_H-\int_{P}^{P_H}P\left(\frac{du}{dP}\right)^2 dP, \tag{2.2}$$

which are evaluated along the measured isentrope $P=P(u)$. By recording using various sets of initial conditions and shock-wave strengths, it is possible to determine the caloric equation of state $E=E(P, V)$ in the region of the phase diagram covered by Hugoniot and/or Poisson adiabatics.

Thus, dynamic diagnostic methods based on general conservation laws make it possible to reduce determination of the caloric equation of state $E=E(P, V)$ to measurement of the kinematic parameters of shock-wave and contact-surface motion, i.e., to registration of distances and times, something that can be done with high accuracy. However, the internal energy is not a thermodynamic potential with respect to the PV variables, and to obtain a closed thermodynamic description of the system it is necessary to know an additional dependence of the temperature: $T=T(P, V)$. In optically transparent and isotropic media (gases, Sec. 4), temperature is measured concurrently with the other shock-compression parameters. Condensed media and metals in particular are generally opaque, so that the optical radiation of the shock-compressed medium is not accessible to registration.

The thermodynamically complete equation of state can be derived directly from dynamic measurements without introducing *a priori* ideas as to the properties and nature of the matter under study.[26,38] Working from the first law of thermodynamics and the empirical relation $E=E(P, V)$, it is easy to obtain a linear inhomogeneous differential equation for $T(P, V)$:

$$\left[P-\left(\frac{\partial E}{\partial V}\right)_P\right]\frac{\partial T}{\partial P}-\left(\frac{\partial E}{\partial P}\right)_V\frac{\partial T}{\partial V}=T, \tag{2.3}$$

the solution of which is constructed by the method of characteristics:

$$\frac{\partial P}{\partial V}=-\frac{P+E'_V}{E'_P}, \quad \frac{\partial T}{\partial V}=-\frac{T}{E'_P}, \tag{2.4}$$

or

$$E=E_0\exp\left[-\int_{V_0}^{V}\gamma(V, E)\,d\ln V\right], \qquad T=T_0\frac{PV}{P_0V_0}\left[-\int_{V_0}^{V}\left(\frac{\partial\ln\gamma(V, E)}{\partial\ln V}\right)_E d\ln V\right]. \tag{2.5}$$

Equations (2.3)–(2.5) are supplemented with boundary conditions: the temperature is specified in the range of

[2)] The results of two-dimensional numerical calculations were used in Ref. 172 for comparison with measurements.

low densities, in which either it is possible to calculate it reliably from theory (cesium plasma; Sec. 3) or the temperature is known from experiment.[39]

The right-hand sides of (2.2) and (2.5) of the $E(P, V)$ or $\gamma(P, V)$ relation that were needed for the calculation were found from experimental data in the form of power polynomials and rational-fraction functions. A Monte-Carlo method was used to determine the accuracy of the resulting solution as a function of the experimental errors and the errors in the initial data, with computer simulation of the probability structure of the measurement process.[38]

The thermodynamic universality of the method has made it possible to construct equations of state for a broad range of condensed media and to use it in studies of the thermodynamics of the nonideal cesium plasma based on experiments in shock[33,40] and adiabatic[34] compression of the saturated vapor.

3. DYNAMIC COMPRESSION OF CESIUM PLASMA

Cesium has the lowest ionization potential, ~3.89 eV, among all the practically accessible elements, and this makes it possible to obtain high charage concentrations n_e at moderate temperatures, thereby ensuring a high value of the nonideality parameter at relatively low energy inputs of the experimental arrangements. This element is therefore the most popular object of nonideal-plasma experiments. Figure 3 shows its phase diagram with the parameter regions accessible to the various techniques. Dynamic generation of cesium plasma has been brought about by adiabatic (state 4) and shock compression of saturated vapors in the fronts of direct (6) and reflected (7) shock waves.

Experiments with dynamic compression of cesium vapor have been performed[33,40,44] in the diaphragmed compressed-air shock tube represented schematically in Fig. 4. The setup, which was ~4 meters long and had an inside diameter of 4.5 cm, was heated to ~700°C to obtain high saturated-vapor initial pressures.[43] The ionizing shock wave formed on expansion of argon, helium, or an argon-helium mixture into the saturated

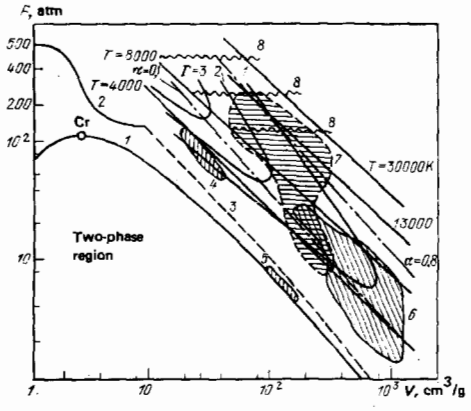

FIG. 3. Phase diagram of cesium. 1) saturation curve; static experiments; 2, 3) after Refs. 17, 19; 4) region of isentropic compression[34,35] from initial states (5), compression by direct (6) and reflected (7) shock waves; 8) electrodetonation[41]; α is the degree of ionization.

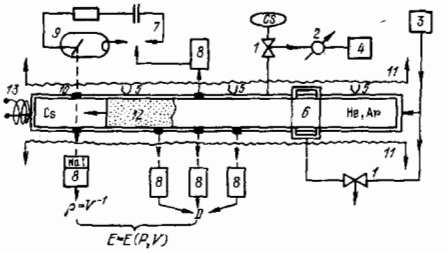

FIG. 4. Diagram of heated cesium shock tube.[33,40,47] 1) air-operated valves; 2) system measuring initial cesium pressure; 3) propelling gas; 4) space with liquid cesium; 5) thermocouples; 6) diaphragm package; 7) x-ray package; 8) photomultipliers; 9) x-ray tube; 10) berryllium windows; 11) electric heater; 12) shock-compressed plasma; 13) electrical conductivity measuring coil.

cesium vapor after the former had been compressed to ~10^3 bar. The parameters of the shock-compressed plasma were raised further by using shock waves reflected from the end of the tube.

Two mechanical parameters that characterize shock compression were recorded independently in each experiment. Optical[33] and x-ray[44] baseline methods were used to determine the velocity of the shock-wave front (to within ~1%) and to monitor the steadiness of the flow of the shock-compressed plasma. The density of the plasma was registered by a pulsed radiographic method based on measurement of the attenuation of "soft" x-rays by the plasma.[45] The ~0.2–0.5 Å wavelength of this radiation was chosen for maximum sensitivity and minimum statistical error of the measuring system.[45] The radiographs obtained in Ref. 45 indicated no appreciable condensation of the shock-compressed cesium[46] and could be used to determine the density of the plasma accurate to 5–10%, as was confirmed by radiography of reliably calculated shock waves in xenon.[40]

Experiments with shock compression of cesium were conducted in the optimum parameter region from the standpoint of nonideality effects (see Fig. 3): $P \sim 1.4$–200 bar, $T \sim 2600$–$20\,000$ K, and $n_e \sim 5 \cdot 10^{15}$–$5 \cdot 10^{19}$ cm^{-3}, where the Coulomb nonideality is at maximum: $\Gamma \sim 0.2$–2.2. It is essential to note that the parameters behind the incident and reflected shock waves overlap partially in the diagram of Fig. 3, at the bottom of which they correspond to a quasiideal plasma. This enables us to make full use of the temperature calculation from (2.3), since the characteristics (2.4), (2.5) of this equation (the isentropes in Fig. 13) lie entirely in the region covered by the experiment, including the region of the weakly ionized plasma $V = 1600$ cm^3/g, where the initial data for Eqs. (2.3)–(2.5) are specified.

The static electrical conductivity of shock-compressed cesium plasma was measured by an induction method (error 20–40%) in a parallel tank-circuit scheme[47] at frequencies of 0.2–2 MHz. An induction coil in the form of a flat spiral was inserted into the end of the shock tube (see Fig. 4) so that its inductance would vary under the action of the plasma formed behind the front of the reflected shock wave. The experiments were conducted at $10 \leq P \leq 150$ bar and $4000 \leq T \leq 25\,000$ K, where the Coulomb interaction dominates, $0.3 < \Gamma < 2$. Unpaired-

atom and atom-correlation effects are weak under these conditions, as are cluster effects, so that it is possible to isolate the Coulomb component of resistivity and compare it to theory (see below, Fig. 16). The absorption coefficient of a xenon plasma was later measured using this apparatus[205] by the technique of Refs. 66, 67, 76.

Where the weakly ionized plasma with strong charge-neutral interaction is of greatest interest, adiabatic compression techniques can be used effectively. Here there are no irreversibility effects, so that it is possible to obtain lower temperatures than in the shock-wave method and rather high densities of the matter.[49,34,35] Here compression must be "smooth" enough so that shock waves do not form, but at the same time it must be "fast" enough to exclude heat-transfer effects. Appropriate arrangements were developed during the 1940s[49] to measure the characteristics of superdense gases at temperatures up to $9 \cdot 10^3$ K and pressures to 10 kbar. Use of these methods in nonideal-plasma physics required significant modification of the designs for the adiabatic-compression devices.

In the two-stage adiabatic tube of Fig. 5, the cesium is compressed[34] by the piston 7 traveling in chamber 5, which can be heated to 1000°C. The absence of the principal entropy-change sources—shock waves and heat transfer—was verified in a special series of methodological experiments with water and argon. Measurement of the pressure and volume of the gas with sensors 2 and 3, together with the isentropicity condition, gives P-V-S data and, on the basis of the relation $(\partial T/\partial V)_S = -(\partial P/\partial S)_V$, the temperature of the plasma. This arrangement made it possible to advance to higher temperatures as compared to the use of a furnace in Refs. 17, 19: $T \sim 3$–$4 \cdot 10^3$K at $P \sim 50$–150 bar, but the electron concentration did not exceed $\sim 10^{18}$ cm^{-3}, with the result that nonideality effects are inconspicuous. The reason for this was that leakage of the cesium through the lightweight piston of this unit compromised the basic advantage of the adiabatic method—its high compression ratios; in this case the compression ratios did not exceed 6, which is close to these characteristic for shock waves. It was possible to avoid this in a single-state tube[35] with a heavy piston having a developed sealing surface. The density of the compressed plasma is measured by pulse radiography, and electrical conductivity by an induction method; it has been proposed that a crusher method be used to register pressures. In the first experiments using this apparatus, the resistivity of the plasma was measured at compression ratios of ~25, pressures up to 330–350 bar, and temperatures of ~6100–4900 K.

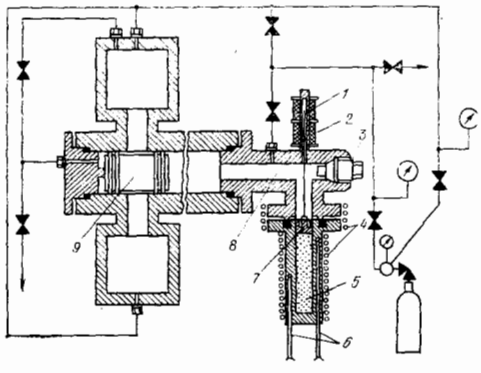

FIG. 5. Diagram of adiabatic tube with free piston.[34]
1) volume sensor rod; 2) volume sensor; 3) pressure sensor; 4) heaters; 5) capsule containing test cesium; 6) thermocouples; 7) working piston; 8) chamber; 9) heavy piston compressing inert gas.

4. COMPRESSION OF INERT GASES BY STRONG SHOCK WAVES

Analysis of experiments with cesium (Sec. 3) indicated a significant contribution of bound states in the dense plasma (see Sec. 5), making it necessary to expand the parameter region studied and to turn to experiments with other chemical elements. This objective required higher shock wave intensities and the use of new high-enthalpy working fluids to generate them.

A shock tube in which the enthalpy of the propelling gas was increased by discharging a battery of condensers with an energy of ~60 kJ was used[50,51] to generate argon, xenon, and air plasmas. Detailed measurements of the thermodynamic (recording of reflected-shock velocities), optical (measurement of increase in radiation intensity), and electrophysical (induction method) properties of plasmas compressed by reflected shock waves were made using this apparatus. Since the generation method used makes it possible to produce a weakly nonideal plasma, $\Gamma \leq 0.2$, at moderate pressures (in the tens of atmospheres), only the first manifestations of plasma nonideality—a small shift of the ionization potential and the photoionization continuum and minor deviations of electrical conductivity from the Spitzer values—were recorded in these experiments.

Significantly higher parameters were obtained using powerful condensed explosives because of their high specific energy capacity and the speed ($\sim 10^{-7}$ sec) of the detonation conversion, which made it possible to produce high-power devices ($\sim 10^{10}$–10^{12} W). It appears that Ref. 52 was the first investigation in which the explosion technique was applied directly to record the shock adiabatic of gaseous argon. A similar technique was then used in Ref. 53 to record shock adiabatics of air at atmospheric pressure with subsequent determination of the dissociation energy of nitrogen on this basis. In a series of studies that followed, explosion shock waves in gases were used to solve various technical[54-55] and scientific[57,55,54] problems. Since the initial pressures of the gas did not exceed 1 bar in studies of this kind, there was not enough time for manifestation of nonideality effects, which, in any event, were not the object of the investigation.

Special experiments to study the influence of nonideality on the physical properties of an explosion plasma were designed in the early 1970s. Inert gases were chosen as objects of study because the elimination of energy expenditure for dissociation and the high molecular weights make it efficient to heat them in a shock-wave front, while the absence of complex molecular and molcular-ion formations and our thorough understanding of the elementary processes greatly facilitate

interpretation of the measured results.

Thermophysical and gasdynamic characteristics of shock waves in dense inert gases were determined by computer[60] with the object of estimating optimum experimental conditions and specifying plasma-generator layouts. It was found (Fig. 6) that the optimum values of the nonideality parameter are obtained at shockwave velocities D of $\sim 9 \cdot 10^5$ cm/sec in argon and $\sim 5 \cdot 10^5$ cm/sec in xenon. Increasing D results in overheating and in an increase in the ionization multiplicity of the plasma, while raising the initial pressure leads to plasma degeneracy. It is important that these optimum conditions can be obtained in a simple linear shock-wave-generating scheme and that either reflected shock waves or geometric cumulation effects must be used to obtain a strongly heated multiply ionized plasma.[61]

In a linear explosion shock tube (Fig. 7),[62-65] an ionizing shock wave is formed on expansion of detonation products of a condensed explosive into the gas to be studied. The use of a specially profiled detonation lens and appropriate dimensioning of the active explosive charge ensured that the detonation front leaving the explosive into the test gas would be one-dimensional and that its parameters would be steady. The total energy release in each experiment was $\sim 3 \cdot 10^6$ J at a power of $\sim 10^{11}$ W, which, of course, destroyed the entire setup and made it necessary to work in specially protected areas with observance of safety measures. The results of photographic, electrophysical, and x-ray measurements indicated a one-dimensional[62-64] and quasistationary flow of the plasma, which ensured inertial confinement of the shock-compressed plasma by the massive walls of the shock-tube.

The velocity of the shock front was measured[63] accurate to ~ 1–1.5% by optical and electrical-contact baseline methods using high-speed motion-picture cameras and ionization sensors. The ionization front coincided within the limits of this error with the light-emitting front of the shock wave and with the position of the hydrodynamic compression shock.

The density of a shock-compressed argon plasma

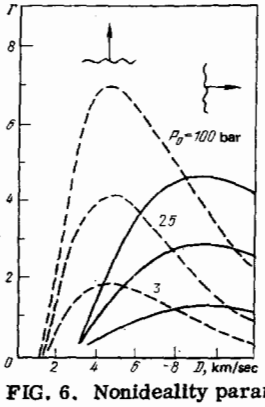

FIG. 6. Nonideality parameters of argon and xenon (dashed) plasmas as functions of shock-wave velocity. The vertical arrow indicates degeneracy and the horizontal arrow overheating of the plasma.

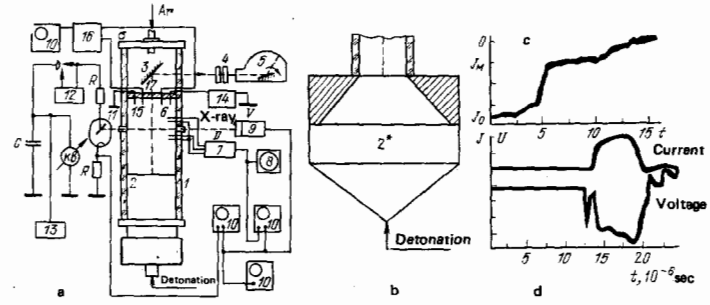

FIG. 7. Diagram of measurements on explosion-type nonideal-plasma generator.[62, 63, 64] a) 1) generator channel; 2) explosive charge; 3) mirror; 4) filter and attenuator; 5) high-speed movie camera; 6) probes for measurement of shock-wave front velocity; 7) power supply to electrical contacts; 8) velocity recording oscillograph; 9) photomultiplier with NaI scintillator; 10) oscillographs; 11) x-ray tube; 12) x-ray control unit; 13) x-ray power supply; 14) dc source; 15) potential and current probes to register electrical conductivity; 16) differential amplifier. The Plexiglas barrier 17 was used in reflected-shock-wave experiments.[65] The design of the active charge 2 was modified in experiments with cumulative devices[68, 69] (b); c) density radiograph; d) current and voltage.

was registered accurate to $\sim 8\%$ by flash radiography (Sec. 3), which does not disturb the flow of the plasma[63] and delivers high temporal ($\sim 10^{-7}$ sec) and spatial (~ 2 mm) resolution.

Because of the transparency of the plasma in front of the shock wave and the small dimensions of the viscous compression shock, the thermal radiation can escape unimpeded from the plasma volume and yields information on the equilibrium temperature and the absorption coefficients of the shock-compressed plasma.[66, 55] Using a brightness method to record temperature (error 5–10%), the intensity of this radiation was determined in Refs. 63, 72 by photometric comparison of time scans of the emission from the shock-compressed plasma and reference light sources: a flashlamp with a brightness temperature of 8600 ± 200 K, a flash capillary light source with $Tl = 39\,700 \pm 700$ K, and a shock wave in air with $T = 11\,800 \pm 600$ K. In accordance with the conservation laws (2.1), simultaneous registration of the front velocity and the density defines the equation of state of the nonideal plasma, $E = E(P, V)$, which, together with the measured $T = T(P, V)$ relation, constitutes thermodynamically complete information on the argon plasma at $P \sim 1.6$–$5.8 \cdot 10^3$ bar, $T \sim 15.5$–$23 \cdot 10^3$ K, $\Gamma \sim 1.3$–2.2, and $n_e \sim 1.5$–$3.5 \cdot 10^{20}$ cm^{-3}.

Electrical conductivity is an important characteristic of a plasma and carries valuable information on its structure and elementary processes. Because the conductivities are high, they were measured[64, 65, 68, 69] by the probe method of Fig. 7, which has high spatial resolution and is relatively simple to work with under the conditions of a single dynamic experiment. To eliminate the distorting influence of electric layers formed at the electrodes by passage of the strong (~ 1 kA) transport current through the plasma, the work was done with a four-point scheme that separated the functions of the measuring electrodes and the ones supplying current to the plasma. The linearity of the volt-ampere charac-

teristics that emerged in the experiments indicates that the diagnostic scheme developed does not violate isothermy ($T_i = T_e$) of the plasma and eliminates the influence of electrode effects—the chief deficiency of probe methods in dense plasma. A typical oscillogram of the transport current and voltage appears in Figs. 7c and 7d, which clearly shows a "plug" of shock-compressed plasma.

Extremely high plasma densities were obtained by compressing near-critical states of xenon in direct and reflected shock waves.[65] For this purpose, a flexiglass barrier was interposed 7 cm from the face of the charge (Fig. 7) to interact with the plasmoid and produce a reflected shock wave that further compresses and heats the xenon plasma. A shock wave was produced in the plexiglas barrier, and its velocity could be recorded to determine[26] the pressure, density, and enthalpy of the xenon after double compression (point 10 in Fig. 8). A noncontradictory description of these thermodynamic data was obtained with a "chemical"[4] plasma model in which the Coulomb interaction was described in a modified Debye approximation and the short-range repulsion by a virial expansion. This thermodynamic model was then used to interpret (Sec. 6) plasma electrical conductivity measurements made under transcritical conditions.

The experiments yielded data on the electrical conductivity of xenon plasma[65] under the strongly transcritical conditions $\rho \sim 1-4$ g/cm^3 ($\rho_{cr} \sim 1.1$ g/cm^3) at the high pressures and temperatures $P \sim 20-110$ kbar, $T \sim 1-2 \cdot 10^4$ K. It is possible in precisely this way to produce plasma under unusual conditions: with densities 1.5 times higher than that of solid xenon and comparable to those of solid metals. The parameter region

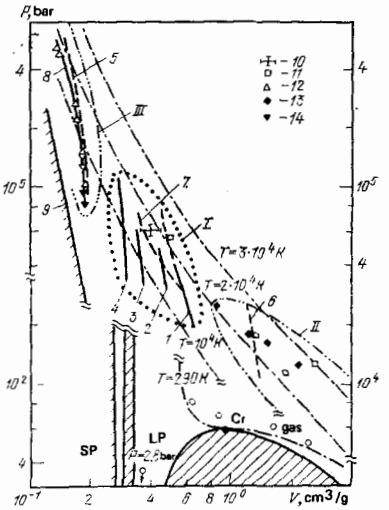

FIG. 8. Phase diagram of xenon. Theoretical adiabatics: 1) $P_0 = 50$ bar; 2) 60 bar; 3) 70 bar; 4) 80 bar; 5) 2.8 bar, $T_0 = 165$ K; 6) $P_0 = 20$ bar; 7) shock adiabatic of secondary compression[65]; 8) calculation from band model[94]; 9) $T = 0$ isotherm. Results of thermodynamic measurements: 10) "reflection" method[65]; 11) Ref. 72; 12) Refs. 94, 8. Data from electrical conductivity measurements: 13) Ref. 64; 14) Refs. 8, 94. SP is the solid phase and LP is the liquid phase.

I studied in Fig. 8 extends from states II of the quasi-ideal low-density plasma to the region III of solid-state densities, which is obtained by dynamic compression of liquid xenon and described by the band theory of solids.

The effort to produce plasma with high nonideality parameters requires experiments to be conducted at relatively low temperatures, $T \sim 20\,000$ K, where the plasma is generally not completely ionized.[34, 35, 40, 42, 63, 64] At the same time, study of multiply ionized nonideal plasma is of considerable interest in that it enables us to investigate the pure Coulomb effects in a strongly overheated medium. The use of reflected shock waves has made it possible to advance into the multiple-ionization region and produce plasmas at temperatures above 20 000 K.[65, 69] The same purpose is served by cumulative blast tubes,[65, 69] the action of which is based on increasing the parameters of the propelling gas in centripetal motion[70] in the conical chamber of Fig. 7, which has vertex angles of $\sim 60-120°$. Shock-wave velocities of 8–15 km/sec have been produced in xenon in this way from initial pressures below 10 atm. This corresponds to highly heated $(3-10) \cdot 10^4$ K, nonideal ($\Gamma \sim 2$) plasma. Leaving the interpretation of these data for Sec. 5, we note that scattering of thermal electrons by the inner shells of ions is significant under these conditions.

Explosion-type generators that produce square shock waves (Fig. 9) of varying intensity and duration have been used to measure the thermodynamic and optical characteristics of plasma at pressures higher than those obtained in shock tubes.[71-73] In this type of apparatus the ionizing shock wave formed on expansion into the test gases (argon, xenon) of metallic or polymeric targets that had first been compressed to $\sim 10^6$ bar. Strong shock waves were set up in the targets with linear explosive propulsion devices[20] the action of which was based on acceleration of flat metal strikers to velocities of 2–6 km/sec by the detonation products. The typical energy releases in these experiments were $(2-30) \cdot 10^6$ J with powers of $\sim 10^{11}$ W.

Two kinematic parameters, the front velocity D and the mass velocity U of plasma motion, were registered simultaneously by electrical-contact and optical baseline methods in experiments using these generators.[71-73]

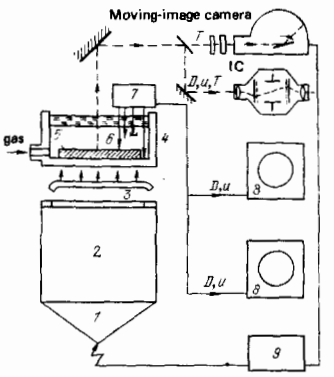

FIG. 9. Diagram of experiments with explosive compression of inert gas plasmas.[72,73] 1) Detonation lens; 2) explosive charge; 3) metal striker; 4) test assembly; 5) target; 6) test gas; 7) electrical contacts and pulse-shaper block; 8) oscillographs; 9) synchronization and detonation block.

Open electrical-contact sensors recorded the front velocity D accurate to ~1% on high-speed oscillographs. The mass velocity U (error 1–2%) was measured with closed sensors of a special design that do not respond to a shock wave in the plasma and operate at the time of arrival of the heavy contact surface between the plasma and the target. In the optical recording technique of Refs. 73–74, a Plexiglas barrier was set up at a certain distance from the target and the emission of the shock-compressed plasma was recorded through it with high-speed motion-picture cameras or image converters, and the manner in which this emission varied permitted interferences as to the motion of the shock wave and the contact surface of the plasma.

Figure 10 shows records of shock adiabatic in argon and xenon in the kinematic variables, clearly showing the internal agreement of data obtained by optical, electrical-contact, and x-ray techniques on explosion shock tubes and square-wave generators that use metal, polymer, and condensed-explosive targets. The results obtained for the equation of state of the nonideal argon and xenon plasmas pertain to a broad range of parameters (Fig. 11): $P \sim 0.3$–40 kbar, $T \sim 5.2$–$60 \cdot 10^3$ K, $n_e \sim 10^{14}$–$3 \cdot 10^{21}$ cm^3, and ρ up to 1.3 g/cm^3, with developed ionization, $\alpha \sim 3$, and strong Coulomb interaction, $\Gamma \sim 10^{-2}$ to 5.2.

The optical properties are of considerable interest for plasma physics, since they enable us to trace the influence of nonideality on the dynamics and energy spectrum of the electrons in the dense disorganized medium. Plasma absorption coefficients $\varkappa_\nu$ have been measured by recording the buildup with time of the intensity of the optical radiation leaving a plane-parallel plasma layer enclosed between a shock front and a contact surface.[66,75,76] Because the photon relaxation time is small compared to the characteristic gas-dynamic time, the spectral intensity $J_\nu(t)$ of the radiation from this layer has the following form in a quasistationary approximation[26]:

$$J_\nu(t) = J_{\nu p}\left(1 - \exp\left\{-\varkappa_\nu\left[1 - \exp\left(-\frac{h\nu}{kT}\right)(D-U)\,t\right]\right\}\right), \quad (4.1)$$

where $J_{\nu p} = J_\nu(\infty)$ is the Planck intensity of the radiation.

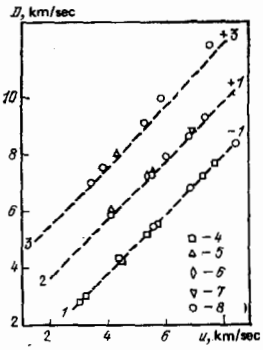

FIG. 10. Shock adiabatics of argon. 1) $P_0 = 0.78$ bar; 2) $P_0 = 5$ bar and of xenon, 3) $P_0 = 10$ bar, registered by various methods: 4) optical[52]; 5) electrical-contact[72]; 6) x-ray[63]; 7) optical[74]; 8) electrical-contact and optical[73]; the dashed lines represent the calculation of Ref. 60. The numbers on the right are the shifts of each curve in the front velocity D in km/sec; u is the mass velocity.

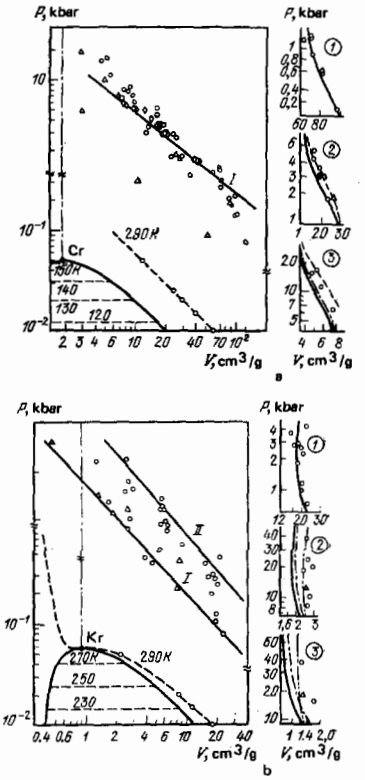

FIG. 11. Phase diagrams of argon (a) and xenon (b). The boundaries of the two-phase region and the critical point Cr are indicated. The dashed lines are the isotherms of the initial states, and the dash-dot lines the V_{cr} isochors. Lines I–II are the single- and double-ionization boundaries. The circles represent the results of dynamic experiments (see Fig. 10). On the left, the experimental shock adiabatics are compared with the results of the theories. The solid curves take into account the interaction of charged particles in the Debye ring approximation[60] and the dot-dash curves also include the interaction of atoms in the second-virial-coefficient approximation[81]; the dashed curves represent the "bounded-atom" model calculation (5.4)–(5.6),[73] and the double dot-dash curves the charge interaction in the model of Ref. 73 with the pseudopotential (5.7).

With the aid of mirrors and an optical system, the optical radiation escaping the plasma is diverted to polarization filters and photomultipliers and the respective signals are recorded on high-speed oscillographs. The plasma kinematic parameters necessary for determination of the absorption coefficients were determined by electrical-contact and optical methods. Emergence of the shock wave from the target into argon resulted in a smooth rise (Fig. 12a) of the luminous emission to luminous emission to saturation in accordance with (4.1). A brightness spike marks the time (and hence the velocity D) of arrival of the front at the transparent obstacle. The cutoff of the emission that follows results from destruction of the obstacle by the massive target in motion at velocity U.

Measured absorption coefficients of light (error ~30%) with a frequency of $5.17 \pm 0.05 \cdot 10^{14}$ sec^{-1} appear in Fig. 18, where each experimental point was obtained by averaging five to ten experiments with two or three independent frequency records each. It is seen that the results of the measurements cover a broad range of plas-

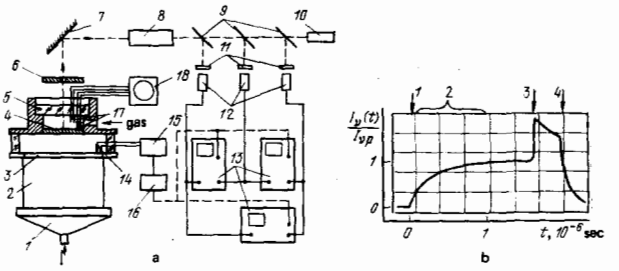

FIG. 12. Diagram of experiment to register absorption coefficient of shock-compressed plasma.[76] 1) Detonation lens; 2) explosive charge; 3) striker; 4) target; 5) transparent barrier; 6) diaphragm; 7) mirror; 8) optical system; 9) semitransparent mirrors; 10) aligning laser; 11) interference filters; 12) photomultipliers; 13) oscillographs; 14) electrical contacts for shock-wave-velocity measurement; 15) pulse-shaping circuit; 16) delay line; 17) electrical contacts for measurement of shock-wave velocity D; 18) oscillograph for measurement of shock-wave velocity; b) oscillogram of experiment of Ref. 76: 1) entry of shock wave into gas; 2) segment with emission buildup; 3) collision of shock wave with barrier; 4) beginning of destruction of barrier by target material.

ma compressions and are in reasonable agreement with the $\varkappa_\nu$ estimates from Ref. 55 and the measurements of Ref. 75, which were corrected for the true values of the plasma temperature.[60]

5. PHYSICAL PROPERTIES OF THE NONIDEAL BOLTZMANN PLASMA

a) Thermodynamic properties. The data of Refs. 17, 19, 34, 40, and 41, which were obtained for cesium plasma, pertain to various regions of the phase diagram (Fig. 3), which overlap to some degree at the boundaries and agree internally within the limits of error of the experiments. Adiabatic-compression experiments[34] made it possible to advance to higher temperatures ($T \sim 4000$ K) as compared to the static measurements of Refs. 17, 19, but were found inadequate for noticeable thermal ionization of the plasma. Under these conditions, the leading interaction is that of the charges with neutral particles, the contribution of which to the equation of state is within the limits of measurement error. The basic conclusion that follows from these experiments[34] is that no phase layering[79,80] due to the "metal-dielectric" transition is present. Experiments in which cesium was compressed by direct and reflected shock waves further broadened the temperature range (to $T \sim 2.6$–$20 \cdot 10^3$ K; Fig. 4) in which the Coulomb interaction is strong, $\Gamma \sim 0.2$–2.2, and determines the physical properties of plasma with developed ionization.

Significantly higher plasma parameters were obtained in experiments with explosive compression of heavy inert gases,[63,72,73] with pressures up to 60 kbar and temperatures to $6 \cdot 10^4$ K; the plasma densities obtained, $\rho \sim 0.4$ g/cm^3 and $n_e \sim 3 \cdot 10^{21}$ cm^{-3}, approached the density of condensed xenon, and they exceeded this density in the experiment of Ref. 69 ($\rho \sim 4.5$ g/cm^3). The characteristic interparticle distances in the plasma[73] were 6–7 Å and comparable to the 3–4 Å dimensions of the ions and atoms, while the largest nonideality parameters $\Gamma \sim 5$ were near the highest values possible (Fig. 1) for a nondegenerate plasma. The experimental data obtained in Refs. 63, 72, 73 for argon and xenon pertain to a region of developed single ($\alpha_{Ar} \leq 0.7$) and double ($\alpha_{Xe} \sim 1.8$) ionization and enable us to move from the gas into the region of condensed densities (see Figs. 1 and 2). The "chemical" model most favored in plasma physics[1,12,195] was used to interpret the results:

$$F(V, T) = kT\left[N_e \ln\left(\frac{n_e\lambda_e^3}{2e}\right) + \sum_k N_k \ln\left(\frac{n_k\lambda_k^3}{eQ_k}\right)\right] + \Delta F_k + \Delta F_{ea} + \Delta F_{aa} + \Delta F_{hs}, \tag{5.1}$$

where, in addition to the usual notation, Q_k is the static sum, e is the electronic charge, and the ΔF are the corrections for nonideality. All thermodynamic measurements[33,40,63,72,73] indicate a distinct trend for the measured (index I in Fig. 13) enthalpy or internal energy to fall below the traditional plasma calculation, in this case the Debye ring approximation in the grand canonical ensemble of statistical mechanics[1,60] (index II in Fig. 13):

$$\Delta F_k = -\frac{\varkappa^3}{24\pi} - \sum_a n_a \ln\left(1 + \frac{Z_a^2\tilde{J}(\xi)}{2}\right), \tag{5.2}$$

$$\varkappa = \frac{2\sqrt{\pi}e}{\sqrt{kT}}\sqrt{\sum_a Z_a^2 \xi_a}, \quad \tilde{J} = \frac{e^2}{kT}\varkappa.$$

$$Q = \sum_n g_n (e^{-\beta E_n} - 1 + \beta E_n). \tag{5.3}$$

Figures 13 and 14 compare the experimental data with various other plasma approximations—the ideal-plasma model $\Delta F = 0$, $Q = 2$, III; $\Delta F = 0$, Q_ν from (5.3), IV; the Debye theory in a canonical ensemble, V,[1,43]; and the Monte-Carlo pseudopotential model of Ref. 14, VI; the relative contributions of other models to the equation of state were analyzed in Ref. 43. The analysis in Ref. 40 indicates that although most of the theoretical models used do not contradict the experimental isotherms of the cesium plasma within the limits of measurement error, they are incapable of a self-consistent description of thermal and caloric information simultaneously. The inert-gas plasma (Sec. 4) corresponds to much larger nonideality parameters, and in this case the traditional plasma models[1,43,63,72,73] contradict not only the caloric but now even the thermal measurements.

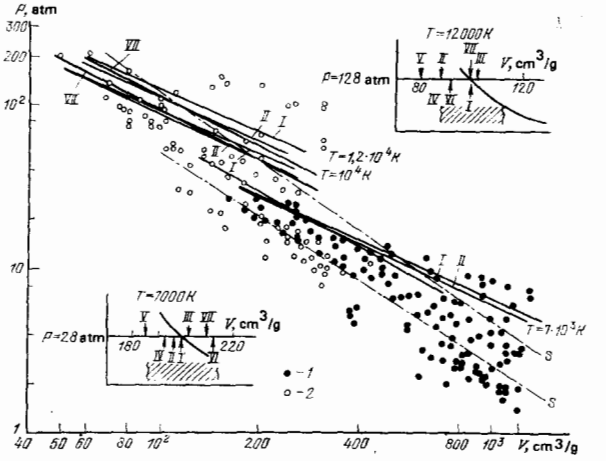

FIG. 13. Results of shock compression of cesium plasma.[40] T) isotherms; S) isentropes. 1) incident shock wave; 2) reflected shock wave.

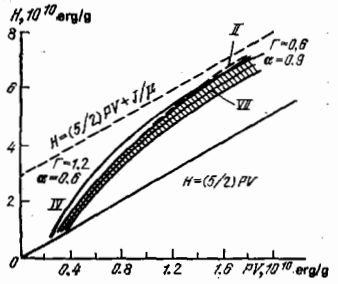

FIG. 14. Isochor $V = 200$ cm^3/g of cesium plasma.[40] The experimental-error strip is shaded.

Analysis of thermodynamic data indicates interparticle repulsion in the strongly compressed plasma, something that cannot be described by the standard[1,43] plasma theories. Even though good agreement can be obtained in the thermal equation of state by modifying the corrections ΔF yielded by these theories, the procedure results in still wider disagreement in the caloric information. It has been established[40,63,72] that a consistent description of thermal and caloric data can be obtained by modifying the contribution of bound states to the thermodynamic functions of the dense plasma—an effect overlooked in most of the plasma models.[1,2,12,43]

Irrespective of this conclusion, experiment indicates that the Debye and similar theories[12,43] give excessively large corrections to the thermodynamic functions for the interaction in the continuous spectrum, and that theories that give nonideality corrections not exceeding the order of the ring approximation in the grand canonical ensemble[1,60] have the best properties of extrapolation into the region $\Gamma \gtrsim 1$.

When the temperature reach the level $T = (10-60)\cdot 10^3$ K, the van der Waals attraction is not significant, and short-range repulsion comes into the foreground. This repulsion was estimated in Ref. 81 within the framework of the second virial coefficient calculated for the Lennard-Jones potential constructed in Ref. 82 from experimental data obtained at moderate temperatures, when the overwhelming majority of the atoms are in the ground energy state. This procedure noticeably improves the agreement with experiment, but leaves a systematic difference at high compressions and indicates the presence of additional repulsion in the system. Actually, at the high temperatures and pressures typical for the experiments,[33,40,63,72,73] many of the atoms and ions are in excited states[196] the short-range repulsion parameters of which exceed the corresponding characteristics in the ground energy state.

In this region of high plasma densities, the average interparticle distances are comparable to the characteristic dimensions of the atoms and ions. This circumstance, along with the strong Coulomb interaction of free charges,[3)] may cause appreciable deformation of the energy levels.

Description of this effect required recourse to a quantum-mechanical model that is not traditional for plasma physics,[73,78] but takes into account the effect of the plasma environment on the discrete spectrum of the atoms and ions in the strongly compressed plasma. In this model, the influence of the environment on the intraatomic and intraionic electrons was described by the effective potential

$$U(r) = \begin{cases} -Ze^2/r & r < r_{av}, \\ \infty & r > r_{av}. \end{cases} \tag{5.4}$$

The characteristic functions and excitation energies were found by using a variant of the Hartree-Fock method[78] in which an integrodifferential equation for the radial part of the wave function $f_{nl}(r)$ is solved numerically:

$$\left[\frac{d^2}{dr^2} + 2V_{nl}(r) - \frac{l(l+1)}{r^2} - \varepsilon_{nl}\right] f_{nl}(r) = \int_0^{r_c} G_{nl}(r, r') f_{nl}(r')\, dr' + \sum_{n' \neq n} \varepsilon_{nl, n'l} f_{n'l}(r), \tag{5.5}$$

where $V_{nl}(r)$ is a self-consistent potential that includes the interactions of the electrons with the nucleus and with one another, and the integral in the right-hand side is the nonlocal (exchange) part of the potential.

Solution of system (5.5) with various r_{av} defines a discrete compressed-plasma spectrum (Fig. 15), and the equilibrium value of the parameter r_{av} is found from the free-energy minimum condition (5.1) $\partial F/\partial r_{av} = 0$, which depends on r_{av} through the statistical sums of the atoms and ions and through the correction for the hard-sphere interaction:

$$\Delta F_{hs} = NkT\,\frac{4-3y}{(y-1)^2}\,y, \quad y = \frac{4\pi}{3} r_{av}^3 N.$$

Unlike the cellular models of a solid,[1] this approximation was constructed within the framework of a quasichemical description technique with explicit allowance for the translational degrees of freedom of the individual particles. The electrons are found to be divided into two kinds and occur both inside and outside of the cells, the volume of which, $(3/4)\pi r_{av}^3$, constitues only a part of the average volume per particle. On comparison of this model with experiments (Fig. 11, index VII in Figs. 13 and 14), we see that it correctly reflects the trend that emerges from experiments by slightly overvaluing

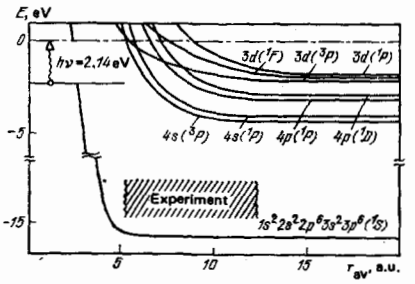

FIG. 15. Quantum-mechanical calculation of energy spectra of compressed argon in bounded-atom model.[73] The region of the experiments of Refs. 73, 76 is shaded; $h\nu = 2.14$ eV is the energy of the light emission registered in the experiments of Ref. 76.

[3)] Under the conditions considered, the intensity of the fluctuating microfields in the plasma is comparable to that of the nuclear field for bound electrons, and this should noticeably affect the physical properties of the strongly compressed plasma.

the effect of repulsion at near-critical plasma densities. The more adequate "soft-sphere" model should evidently be used under these conditions.[1]

The need to consider variations of the discrete electron spectrum in dense-plasma thermodynamics is also pointed up by experiments in shock compression of liquid argon and xenon at pressures up to ~1 Mbar.[210] Interpretation of these measurements[210] required recourse to Wigner-Seitz quantum-mechanical models and associated plane waves.[1]

The arbitrariness with which the particles are classified as free and bound is a property of quasichemical description of plasma under conditions of strong nonideality. Thus, an effect treated as distortion of the excited-state contribution may, with a different classification into kinds of particles, be treated as a manifestation of the quantum nature of the electron-ion interaction at short distances. In Ref. 73 this interaction was described with the pseudopotential

$$\Phi_{ie}^{*}=\frac{z_i e^2}{r}\left[1-\exp\left(-\frac{r}{\sigma}\right)\right],\quad \Phi_{ee}=\frac{e^2}{r},\quad \Phi_{ij}=\frac{z_i z_j e^2}{r}, \qquad (5.6)$$

on the basis of which a semiempirical model of the nonideal plasma was constructed using local electroneutrality conditions.[84] By setting the only parameter of the model—the depth of the pseudopotential $\Phi_{ie}^{*}(0)$—equal to the energy that classifies the particles as free and bound, it is possible to arrive at a noncontradictory description of all presently known thermodynamic experiments.[73]

b) Electrical conductivity is the most instructive and easily observed characteristic of a plasma, determining its dissipative heating and interaction with the electromagnetic field. Other circumstances that have attracted the attention of experimenters to this problem are the relatively simple and thoroughly refined methods of registration and the possibility of making electrophysical measurements under a very wide variety of experimental conditions. Electrical-conductivity measurements made under stationary and quasistationary conditions[42,182-185] have made it possible to record metallization of plasma at supercritical pressures, but the conductivity values measured on the saturation line exceed the theoretical estimates by 5–6 orders of magnitude. This effect was linked in Refs. 186, 187 to a strong "charge-neutral" interaction, which gives rise to the formation of heavy positive clusters whose role diminishes with increasing temperature. Dynamic methods are especially effective for generation of high-temperature plasma with developed ionization, in which case the Coulomb interaction predominates. Some of the material parameters obtained in this region are shown in Fig. 16, which is of schematic nature for experiments with the alkali metals in view of the difficulty of separating the Coulomb contribution from the measured electrical conductivity.

The nonideality parameters obtained in the early experiments[5] did not exceed $\Gamma\sim 0.2$–0.3, and the measured conductivities were in agreement[3,86] with calculations based on the kinetic equations or the method of time correlation functions.[3,15] As nonideality increases, considerable difficulty is encountered in validating the

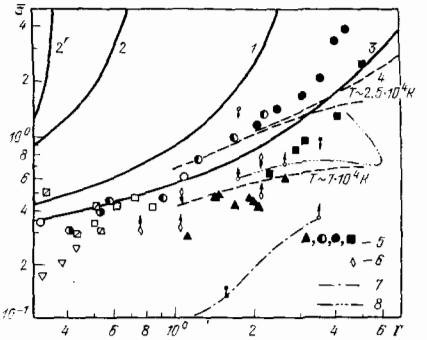

FIG. 16. Dimensionless electrical conductivity $\bar{\sigma}=\sqrt{1+\bar{z}\gamma(z)}\times(\sigma/\omega_p)\Gamma(\omega_p=\sqrt{4\pi ne^2/m}$, $\gamma(z)$ is a correction factor[85]) as a function of the nonideality parameter. Theories: 1) Ref. 85; 2) Ref. 88; 2') Ref. 89; 3) modified Ziman approximation (5.7)–(5.8); the dashed lines represent the calculation with the pseudopotential (5.9) for various temperatures; 4) Refs. 93, 95. Experiment: 5) shock compression of argon, xenon[64,65,68,69]; 6) of cesium[47]; the other points were obtained with arcs and discharges (see Ref. 69 for details); 7) slow electrodetonation of cesium[41]; 8) isobaric heating of cesium.[42] The arrows indicate the changes of $\bar{\sigma}$ due to the uncertainty of separation of the Coulomb component.

original kinetic equations and the methods for their solution. For example, the strong collective interaction in dense plasma makes clear-cut separation of the characteristic elementary-process times impossible. Correction for bound states in a partially ionized plasma is a special problem[87] in the absence of appropriate kinetic equations and transport cross sections that would permit use of semiempirical methods. As a result, the calculations are of extrapolative nature and in particularly urgent need of experimental verification.

Figure 16 shows several such extrapolations. Curve 1 corresponds to Spitzer's theory,[85] which is based on numerical integration of the Fokker-Planck kinetic equation. Application of a diagram technique (ring and ladder fragments were used) to the equations of motion for temporal Green's functions in Ref. 88 yielded a kinetic equation that takes into account the interparticle interaction in the first order in Γ (curve 2). Allowance for collective effects in the Coulomb interaction was based in Ref. 89 on the Fokker-Planck equation for a single-particle function, where all moments and distribution functions enter into the collision integral (curve 2').

Dynamic methods have made it possible to measure[64,35,47,51,65,68,69] the static ($\omega\ll\omega_p=\sqrt{4\pi ne^2/m}$) electrical conductivity of a plasma in a broad range of nonideality parameters from $\Gamma\sim 0.3$, where the differences between the theories are minor and numerous experimental data are available,[5] all the way to the region of extremely high $\Gamma\sim 5$–10, where most theoretical approximations disagree and where the results of experiments form a basis for construction of physical models of electron transport in dense disordered media.[90-93] This range has been investigated with the aid of various media—cesium,[47,35] air,[51] neon, argon, and xenon[64,65,69] in parameter ranges that partly overlap each other and other measurements. It is important

that, together with electrical-conductivity measurements, thermodynamic and gasdynamic measurements have been made for plasmas of these elements (Secs. 3, 4), so that more definite inferences can be drawn as to the physical conditions of the shock-compressed plasma.

The highest plasma parameters (P up to 110 kbar, $n_e \sim 10^{21}$ cm^{-3}, $T \sim 1-2\cdot 10^4$ K) have been obtained[64,65] for xenon (Fig. 8), in which case the experiments covered supercritical densities $\rho \lesssim 4$ g/cm^3 and continuously followed the behavior of electrical conductivity from the low-density states II, which can be described by plasma models,[68-92] up to the region of solid-state densities III obtained by shock compression of liquid xenon,[94] where the shock compressibility is described by the band theory of solids[8,94] and the conductivities are in agreement with semiconductor models.[93,95]

In the aggregate, recent experimental data (Fig. 16) definitely indicate that the measured conductivities are below those from Spitzer's theory,[85] whereas the more rigorous theories[88,89] predict higher conductivities than those of Ref. 85. The existing quantitative disagreement between various groups of experiments in Fig. 16 is due both to the peculiar behavior of the high-temperature plasma and to the existing disagreement of the primary data, as well as to the difficulties of separating the Coulomb component in weakly ionized plasma. This last circumstance is most characteristic for experiments with alkali metals,[42] where the neutral-particle contribution is especially large because of the large cross sections for scattering of electrons by atoms in the ground and excited states[48] and the inadequate degree of ionization. This means uncertain separation of the Coulomb component $\bar{\sigma}$ from the results of low-temperature measurements,[42] where it ranges into the hundreds of percent (see the arrows in Fig. 16).

Use of strong shock waves (Sec. 4) yielded[64,69] a plasma with a high degree of ionization for which separation of the Coulomb component is no problem; this simplified interpretation of the experiments by reducing the uncertainty as to the thermodynamic composition and cross sections of non-Coulomb processes. Results obtained by dynamic methods can be classified arbitrarily as "low-temperature" ($T < 2\cdot 10^4$ K[64,65]) and "high-temperature" ($T > 2\cdot 10^4$ K[69]) data. Here the low-temperature points correspond to extremely high densities $\rho \sim 4$ g/cm^3, which are close to the electron-component degeneration boundary and where the Coulomb interaction is strong, $\Gamma \sim 6-10$, while plasma with developed single and double ionization forms in the high-temperature region. Figure 16 shows that the results obtained with various gases agree with one another and make it possible to trace the influence of the Coulomb interaction on electrical conductivity over a broad and continuously varying range of nonideality parameters $\Gamma \sim 0.3-10$.

The lower electrical conductivity of the nonideal plasma as compared with data from the asymptotic theories may result[96] from an increase in the Coulomb collision cross sections as compared with theoretical estimates, which predict anomalously small ($\lesssim 10^{-8}$ cm) screening radii at $\Gamma \gtrsim 1$. It appears[64] that the interaction is renormalized in the nonideal plasma and that the charge correlation radius is of the order of magnitude of the interparticle distance, much as in the case of metals and doped semiconductors.[95] The corresponding model[95] used to describe electron scattering on impurity centers of semiconductors is marked with the index 4 in Fig. 16.

The model proposed in Ref. 92 to describe the results of the experiments in Refs. 64, 65 described the ionic correlations in the Ziman approximation,[97] which was borrowed from the theory of liquid metals and semiconductors, and the charge scattering was calculated in the Born approximation with screening by a Coulomb potential. In the τ approximation[97] we have for the electrical conductivity

$$\left.\begin{aligned} \sigma &= \frac{4e^2}{3\sqrt{\pi}\,m_e}\,\xi\int_0^\infty \frac{x^{3/2}\exp(-x)\,dx}{\nu_{ea}(x)+\sum\gamma(z_j)\,\nu_{ei}(x)}, \\ \nu_{ej} &= \frac{\sqrt{2}}{16\pi}\,\frac{1}{n_j\sqrt{m_e}\,\varepsilon^{3/2}}\int_0^{4\varepsilon/z_j e^2} |u_j(q)|^2\,a_j(q)\,q^3\,dq, \\ x &= \frac{\varepsilon}{kT}, \end{aligned}\right\} \qquad (5.7)$$

where ξ is an activity related to the electron concentration within the framework of the Debye ring approximation by the expression $\xi = n_e[1+(\gamma/2)]^{-1}$,[48,60] and expressions that follow from the ring approximation are used for the structure factor a_j and the form factor and the pseudopotential u_j:

$$a_j(q) = 1 - \frac{4\pi e^2 z_j\left(\sum_k z_k n_k\right)}{kT(q^2+\varkappa_0^2)}, \quad u_j(q) = \frac{4\pi z_j e^2 n_j}{q^2+\varkappa_0^2}. \qquad (5.8)$$

These relations have the correct Spitzer asymptotic form as $\Gamma \to 0$ and acceptable extrapolation properties, and do not have nonphysical divergences, describing satisfactorily the "low-temperature" experiment of Fig. 16 all the way up to extremely high Γ.

Fairly low ($T < 4\cdot 10^4$ K) temperatures are characteristic of nonideal-plasma experiments, since they are oriented to obtaining developed Coulomb nonideality, which decreases with rising temperature. The use of cumulative shock tubes and reflection of shock waves from obstacles has made it possible to advance[69] into a region of much higher temperatures and to obtain a highly heated multiply ionized plasma with developed Coulomb nonideality, $\Gamma \sim 1-5$. The electrophysical properties of this plasma were to a considerable degree unexpected,[69] since they indicate the lack of similarity of the Coulomb component of the nonideal plasma—the dimensionless electrical conductivity of the high-temperature plasma in Fig. 16 is found to be lower than that of the high-temperature plasma at the same values of the Coulomb nonideality Γ. This result is in qualitative contradiction to the models of Refs. 98 and 99, which simplify to the limit the description of similar states in the plasma by forced limitation of the minimum impact parameter to the thermal deBroglie wavelength of the electron and predict the opposite behavior of the reduced electrical conductivity with temperature.

Analysis of high-temperature data[69] indicates that this effect is caused by the non-Coulomb nature of the scat-

tering of high-energy electrons by heavy ions. In fact, the amplitude of the Coulomb scattering $f_C \sim e^2/kT$ decreases with increasing temperature and is comparable to the characteristic dimensions of the ions, $Q_{X_e} \sim 4$ Å, so that high-energy conduction electrons may, as they are scattered, approach quite close to the nucleus, where the interaction potential is no longer purely Coulomb and is distorted by inner electron shells. In this neighborhood of the nucleus, the potential is stronger than the external ionization potential, and this is what increases the scattering cross section and, consequently, produces the experimentally observed (Fig. 16) relative decrease in electrical conductivity. Screening, which lowers the external ionic potential, is a factor favoring the appearance of this effect in the nonideal plasma.

The non-Coulomb-scattering effect was described in Ref. 69 with a pseudopotential model in which the conductivity was calculated in Frost's approximation,[86] while the electron-ion interaction was described by an effective pair potential[100] that takes account of ion composition:

$$V(r) = -\left[\frac{z}{r} + \frac{(z_{\text{nuc}} - z)}{r}\exp(-\beta r)\right]\exp\left(-\frac{r}{r_D}\right), \quad \beta = \frac{1.8 z_{\text{nuc}}^{4/3}}{(z_{\text{nuc}} - z)}. \tag{5.9}$$

The potential (5.9) was used in numerical solution of the Schrödinger equation with subsequent calculation of the transport scattering cross sections by the partial-plane-wave method; this made it possible to describe satisfactorily the electrical-conductivity decrease experimentally observed in the high-temperature plasma.

c) The optical properties of high-density plasma have recently come under more intensive study, since they are important in crucial applications[3-5,8,9] and carry important information on the dynamics and energy spectrum of the nonideal plasma. The theoretical concepts that have been developed[101-108] pertain to rarefied plasma, where the elementary processes are easily separated and the influence of the plasma environment reduces to broadening of the spectral lines and shifting of the photorecombination thresholds, which have been registered reliably in numerous rarefied-plasma experiments.[50,51,55,59,101,209]

The few data available for dense plasma ($\Gamma \leq 0.2$–0.3, $n_e < 10^{18}$ cm^{-3})[102-104] were obtained using apparatus with electrical heating of the plasma and are in many ways contradictory, although they indicate that the continuum emission exceeds the calculated data as the density of the plasma increases. Further, plasma screening[105] and strong fluctuating microfields[106] may significantly distort the near-threshold region of the spectrum, lowering the recombination-emission intensity of the dense plasma.[103,104,107,207,208]

The spectral region near the photoionization threshold has recently been attracting increased attention, since disappearance ("nonrealization") of some of the highly excited states near the continuous spectrum of the dense plasma has been predicted for this region.[103] Among other things, records of the mercury discharge spectrum have been interpreted from this standpoint.[104] In dynamic experiments, the near-threshold region of

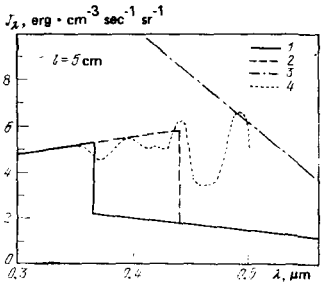

FIG. 17. Emission from hydrogen (90%) argon (10%) plasma.[51] 1) calculation of J_λ with allowance for free-bound and free-free transitions in the fields of the ions, photoattachment of electrons to H^- and the recombination continuum of Ar; 2) Inglis-Teller photorecombination threshold shift[101]; 3) blackbody emission ($T = 145\,000$ K); 4) experiment.[51]

the spectrum has been thoroughly investigated in hydrogen plasma in an electric-discharge shock tube,[51] where no significant anomalies in the plasma emission were observed (Fig. 17) at $n_e \sim 8 \cdot 10^{17}$ cm^{-3} and $T \sim 14\,500$ K, and the shift of the photorecombination threshold was described by the Inglis-Teller formula.[101] Similar results were obtained later[206] with a hydrogen arc at $n_e \sim 2$–$6 \cdot 10^{17}$ cm^{-3} and $T \sim 15 \cdot 10^3$ K.

Plasma-nonideality effects stand out in stronger relief in the case of argon.[76] A broad and continuous range of parameters has been obtained, from the previously studied states[102] with $n_e \leq 10^{18}$ cm^{-3} and $\Gamma \leq 0.3$ to extremely high parameters, $n_e \sim 2 \cdot 10^{20}$ cm^{-3} and $P \sim 5000$ bar, where the strong ($\Gamma \sim 1.6$) nonideality causes a qualitative change in the radiation characteristics of the plasma (Fig. 18). The absorption in free-free electron transitions in the fields of the ions is described by the Kramers formula[101] (Curve 1). Allowance for screening results in lower absorption (Curve 3). To obtain the total absorption coefficient (curve 2), it is

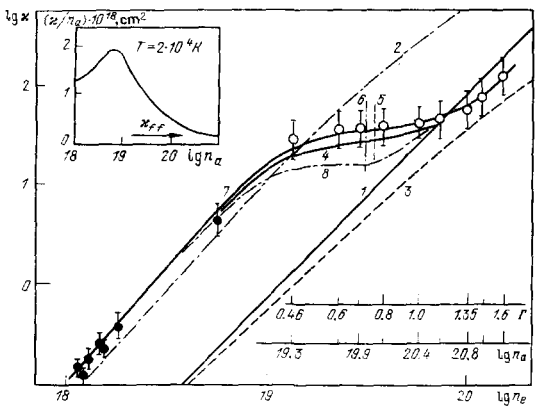

FIG. 18. Absorption coefficient of shock-compressed argon plasma. Open circles—data of Ref. 76; dark circles—data from other studies. Calculation: 1) free-free transitions (κ_{ff}); 2) photoionization taken into account; 3) free-free transitions with correction for plasma screening; 4) calculation from bounded-atom model[73]; 5, 6) estimate from results of Refs. 55 and 75; curve 7 joins the experimental points reduced to the radiation frequency $h\nu = 2.14$ eV, temperature $T = 2 \cdot 10^4$ K; 8) claculation by Hartree-Fock-Slater method[113]; a) specific coefficient of absorption.

necessary to consider the photoionization of bound states in addition to the free-free transitions.[111] We see that experimental data from the low-density region agree with numerous earlier measurements[102] and confirm the tendency in which the registered radiation exceeds calculations. As the plasma is further compressed, the specific absorption coefficient $\varkappa_\nu/n_e$ decreases monotonically and is an order of magnitude below the traditional plasma calculation[101] and close to the values determined by free-free transitions alone.

The experimentally observed "transparentization" of plasma was interpreted in Ref. 76 as a result of deformation of the electron energy spectrum of the atoms as they are compressed as a result of the action of surrounding particles on them. In dense plasma, the interparticle interaction makes the intraatomic potential shorter-range, and this results in a finite number of discrete energy levels and successive transitions of highly excited states to the continuous spectrum with increasing plasma density. This disappearance of some of the excited energy levels eliminates the photoionization-absorption mechanism from these states and causes the observed[76] decrease of the absorption coefficient.

The bounded-atom model (5.2)–(5.5), which describes the thermodynamics of the strongly compressed argon plasma (Sec. 5),[73,78] was used in Ref. 76 to describe this effect. Fig. 15 shows the type of deformation of the energy spectrum, indicating the experimentally recorded[76] range of quantum energies $h\nu \sim 2.14$ eV that can cause photoionization from the respective energy states. We see that this model reflects the "transparentization" of the plasma during compression that has been recorded in experiments. The results of these experiments can also be described satisfactorily (Fig. 18) by a quantum-mechanical model[113] that takes into account the deformation of the spectrum in the Hartree-Fock-Slater approximation, where a quasihomogeneous electron-gas model is used to describe the exchange interaction.

6. ISENTROPIC EXPANSION OF SHOCK-COMPRESSED METALS

The shock-wave technique used in Secs. 2–4 enables us to produce high pressures and temperatures in compressed media, whereas the range of low densities (including the saturation curve and the neighborhood of the critical point in the case of metals) remains inaccessible to these methods. Steady-state experiments at normal pressures and temperatures below 2500 K determine the heat capacity and isothermal and adiabatic compressibilities, as well as the entropy and density jumps that occur during melting.[116,117] The melting curves of metals and the general form of the phase diagram have now been determined[116] at pressures up to 50 kbar and their isothermal compressibilities up to 300 kbar.[117] The properties of metals are determined from absolute records of the shock and isentropic compressibilities of compact and porous specimens in the pressures into the tens of megabars.[27-30]

This leaves unexplored a broad and practically important part of the phase diagram (see Figs. 1 and 2) that is characterized by wide diversity and extreme complexity of description of the physical processes. In this region we have plasma that is nonideal with respect to a broad spectrum of interparticle interactions, a dense hot metallic liquid on expansion of which the degeneracy of the electron component is lifted and that component recombines, a "metal-dielectric" transition, and high-temperature vaporization of the metal into the gaseous or plasma phase. The presently available information on these processes is extremely limited and exists in the form of semiempirical estimates and a few measurements. It is sufficient to note that of the more than 80 metals of the periodic system, the critical-point parameters have been determined only for the three lowest boiling-boiling elements,[17,19,118] not to mention any more detailed information on the form of the phase diagrams of metals at high pressures and temperatures.

The isentropic expansion method,[119-125] which is based on generation of a dense plasma on isentropic expansion of condensed matter that has been compressed and irreversibly heated in a shock front, permits some progress into the region of low densities and high pressures.

With the object of determining the capabilities of dynamic methods for isentropic generation of nonideal plasma, energy releases in the condensed phase that results during adiabatic decay in melting and vaporization in the decompression wave were calculated in Ref. 126. Semiempirical estimates[118,127] (see Table II) indicate that the critical temperatures of the metals are quite high because of collectivization of outer electrons, and are in many cases comparable to their ionization potentials.[1,118] Therefore metal vapors on the right-hand branch of the binodal curve are evidently thermally ionized, while high-temperature vaporization of metals corresponds to direct transition to the nonideal plasma state without going through the unionized-gas region, in contrast to the elements studied thus far. This may be reflected in the kinetics of the high-temperature phase transitions,[129] and may also sharply distort the usual form of the phase diagram of the substance, leading to the appearance of additional phase-separation regions and new and exotic phase transitions

TABLE II. Parameters of critical points and pressure P_n on shock adiabatics of metals of various porosities that result in vaporization, condensation, and attainment of near-critical states: 1) Metals; 2) critical point; 3) kbar; 4) g/cm³; 5) cal; 10) mole · K; 6) porosity; 7) vaporization; 8) critical point; 9) condensation.

Metals		Ni		Al		Cu		Pb	
		critical point							
T_c, K		10300		8000		8400		5000	
P_c, kbar		9.1		4.5		7.5		1.9	
ρ_c, g/cm³		2.2		0.6		2.4		3.2	
S_c, cal/(mole · K)		36.5		33.5		35.3		49.8	
		$m=1$	$m=3$	$m=1$	$m=3$	$m=1$	$m=4$	$m=1$	$m=2$
porosity									
vaporization	P_H, Mbar	3.8	0.3	1.7	0.2	2.7	0.2	0.7	0.1
critical point		7.3	0.5	4.4	0.5	7.5	0.7	1.9	0.4
condensation		20	1.9	10	2.7	20	3.9	5.0	1.3

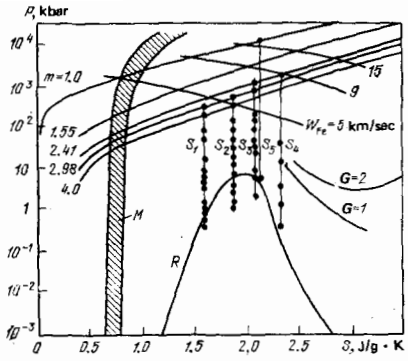

FIG. 19. Entropy diagram of copper. M, R—melting and boiling boundaries; m—shock adiabatics for various porosities, S—expansion isentropes, W—deceleration curves of iron strikers. The dark circles represent the experiments of Refs. 121–125.

(Sec. 7). Entropy-criterion estimates[26] of the energy releases that result in phase transitions during adiabatic expansion of metals indicate[126] (Figs. 19 and 20 and Table II) that to produce transcritical conditions in the decompression wave it will be necessary to generate shock waves of extremely high intensity at the limit of the energetic capabilities of chemical explosives.[20,23] The necessary shock-wave amplitudes can be reduced significantly[119] by using porous targets, which increase the shock-compression entropy more efficiently.

The few experiments performed thus far to record the dispersal of matter under the action of shock waves can be classified into two groups on the basis of the type of physical information obtained in them. Experiments of the first group[130,131,124] are based on Zel'dovich's idea[119,26] of determining the shock-compression entropies of solids by recording the final states of the expanded matter. In experiments of the second group[120-123,125] decompression isentropes were recorded in detail over the entire intermediate parameter region from the solid state to the plasma or gas.

After the passage of extreme-intensity shock waves

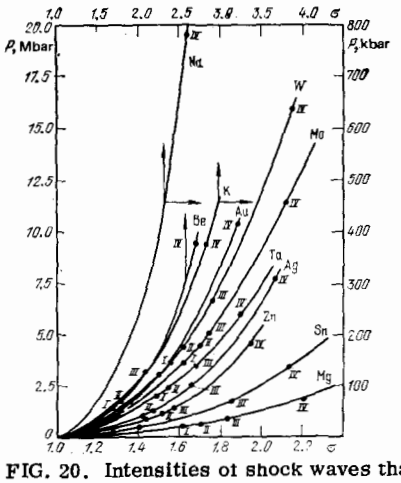

FIG. 20. Intensities of shock waves that cause melting (beginning and end of melting I and II, respectively), boiling (III), and attainment of critical point (IV) in isentropic decompression wave,[126] $\sigma=\rho/\rho_0$.

through the matter under study, the expanded medium enters the state of an ideal gas or plasma,[26,119] the entropy of which (which is the same as the entropy of shock-compressed matter) can be calculated in simple fashion from the measured temperatures, pressures, or densities. The method cannot yet be used in this form owing to the great difficulty of producing states with the necessary high entropy by shock compression. In the case of shock waves of lower intensity, the final states are in the solid or liquid phase, and this has made it possible to use[132] a photoelectric technique to register the residual temperature of copper and, on this basis, to find[133] its entropy and temperature at pressures up to 1.8 Mbar. In Ref. 128, the entropies of sodium, strontium, barium, and uranium were determined by optical adsorption measurements of the fraction of metal vaporized under the action of short shock waves with $P\sim 0.2$–3 Mbar that were generated by thin (0.1–1 mm) strikers moving at velocities of 2–6 km/sec. Entropy analysis[126] shows that shock waves of these moderate intensities can cause appreciable vaporization of metals only by expanding them to extremely low pressures, and this prompted experiments in a vacuum of $\sim 10^{-5}$ torr.[128]

Adsorption measurements made under strongly inhomogeneous flow conditions[128] made it possible to find the degree of vaporization of a metal by relating it to the entropy of shock-compressed metal on the basis of qualitative arguments as to the kinetics of the nonequilibrium vaporization process. In a later series of studies, qualitative notions of vaporization and ionization in the decompression wave were used to analyze high-velocity collisions of solids and to form fluorescent barium clouds in outer space with the object of studying the earth's magnetosphere.[134]

Measurements of the expansion velocity W of lead in air at $P_0=1$ bar after passage of shock waves with amplitudes of 0.4–3 Mbar were used in Ref. 124 to study vaporization in decompression waves. The deviation registered in Fig. 21 from the "velocity doubling" rule constitutes experimental evidence of the vaporization effect. The pressure at which the lead began to vaporize[124] on one of the isentropes determined its point of intersection with the phase boundary, for description of which estimates[128] based on thermodynamic similarity principles were used. These estimated entropy values were then used to improve the semiempirical equations of state of liquid lead. The data obtained in Ref. 124 yield interesting information on the vaporization and condensation kinetics of metals during adiabatic expansion. It is important for kinetic analysis that isentropic expansion presents a unique opportunity that is not offered in most other cases[135]: that of penetrating into the region of absolute instability of the single-phase system, $(\partial P/\partial V)_T>0$, by nonstatic variation of the pressure, since at the critical point, where $(\partial P/\partial V)_T=0$, the value of $(\partial P/\partial V)_S$ remains negative, just as within the spinodal. In this case, the kinetics of lifting of the nonequilibrium state is nonactivative and determined chiefly by heat transfer, and, as estimated in Refs. 129 and 135, admits of supersaturation by several degrees under the conditions of the experiment.

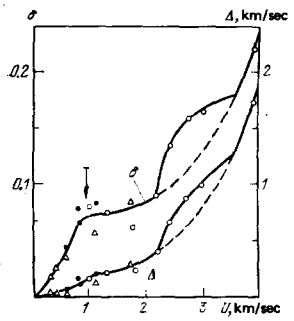

FIG. 21. Deviation from velocity "doubling" law on isentropic expansion of lead into air at atmospheric pressure.[125] Equilibrium and metastable (dashed lines) expansions; the plotted points represent experiments. The arrow marks melting in the unloading wave.

Analysis of the decay kinetics of a metastable metallic liquid showed[129] that because of the pronounced thermal ionization of the metal vapor on the binodal, the metastable phase contains a significant number of charges that are effective condensation centers, giving phase relaxation times of the order of magnitude of 10^9 sec under the conditions of the experiments in Refs. 120–125. The measurements of Refs. 120–125, 130, 131 confirm this viewpoint (Fig. 21), indicating a quasiequilibrium nature for high-temperature condensation of metals. To obtain further clarification of this question, a series of experiments was performed[124] to record the velocity of dispersal of metal into low-pressure air and to analyze the impact of lead vapor on a copper screen. In the equilibrium case, a shock wave with $P = 0.73$ Mbar formed in the copper, while impingement of superheated lead would produce twice that pressure.

Mention should be made of another series of studies of the dispersal of matter after passage of shock waves through it.[130, 136, 178] A converging conical-wave technique used in Ref. 130 gave two points for the expansion of uranium and copper in atmospheric-pressure air. The equation of state was corrected on the basis of these data,[179] but it does not have the correct asymptotic behavior as $V \to \infty$. Results on the soft-obstacle reflection of shock waves in porous copper are reported in Ref. 136, whose authors were interested chiefly in problems of two-phase gasdynamics.

Experiments of the second group[120-125] with decompression adiabatics were based on recording not only of the final, but also of intermediate states that arise during isentropic expansion of matter (Fig. 22). A shock wave propagating through the test substance M compresses it and heats it irreversibly to state a. Emergence of

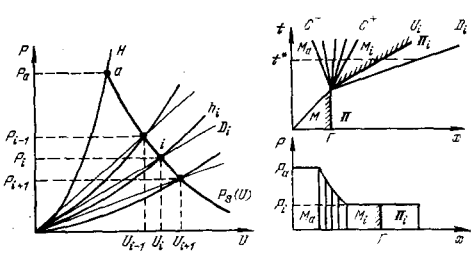

FIG. 22. Schematic diagram of adiabatic-expansion experiments of Refs. 120–126.

the shock wave at the interface Γ with the dynamically softer obstacle II results in formation of a centered Riemann wave C^+C^-, in which the shock-compressed matter expands adiabatically from state a into state i. This expansion of the metal generates a shock wave propagating at velocity D_i in the obstacle. Registration of D_i makes it possible to determine the pressure and mass velocity of motion of the obstacle from the known shock adiabatic h_i—results that agree with the corresponding characteristics of the expanding metal by virtue of continuity[26] at the contact boundary Γ.

By using obstacles of different dynamic rigidities and recording the P and U generated in the process, it is possible to follow the variation of the expansion isentrope $P = P_S(u)$ continuously from states on the Hugoniot adiabatic to lower pressures and temperatures. The use of propelling systems with various powers makes it possible to vary the entropy increment in the shock wave and thereby to investigate various isentropes that cross a selected region of the phase diagram. A transition from hydrodynamic P-u to thermodynamic P-V-E variables can be made by evaluating the Riemann integrals (2.2) that express the conservation laws for the particular type of self-preserving flow.

Three expansion isentropes of shock-compressed uranium were recorded by the "obstacle" method in Ref. 120, which made use of linear and spherical explosive systems. The experiments were performed for the most part in the liquid phase, and the neighborhood of the critical point and the two-phase and plasma regions were not studied, so that the authors could use only qualitative estimates to describe the trend of the isentropes in the low-pressure region.

The adiabatic expansion of lead and copper, which were prepared as fine powders to enhance dissipation effects, was the subject of a systematic series of studies.[121-125] Here special attention was given to the plasma region of the parameters, which was reached by using gases compressed to 1–50 bar as obstacles, while the metal was brought to elevated densities and pressures by using "soft" condensed obstacles (the light metals Al and Mg, Plexiglas, polyethylene, Teflon, and various foamed plastics).

The results of thermodynamic calculations of the shock adiabatics of argon and xenon with consideration of multiple ionization, electron excitation, and Coulomb nonideality were used to determine the dynamic parameters of low-pressure gaseous obstacles.[60] The thermodynamic calculations become less reliable at elevated pressures and velocities, so that it was necessary in this case to use the experimental records of Sec. 4 for the shock compressibility of the dense plasma, and, in some experiments, to make simultaneous independent records of the wave and mass velocities of the shock-compressed plasma.

The experimental data of Figs. 23 and 24 indicate that the adiabatic expansion process covers a very broad range of parameters (four orders of magnitude in the pressure and two in the density), extending from the strongly compressed metallic liquid, where the ions

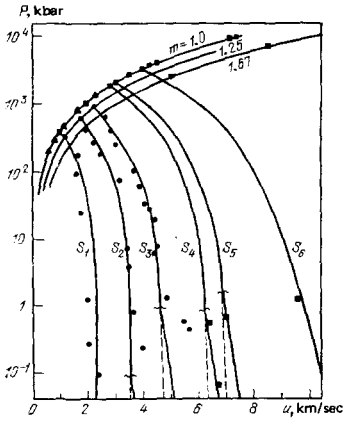

FIG. 23. P–u diagram of lead.[125] m—shock adiabatics for various porosities, S—expansion isentropes. The dashed lines are the metastable branches, and the circles, triangles, and square represent experiments.

are disorganized and the electrons are degenerate, to the quasilinear Boltzmann plasma and rarefied metal vapor. Various poorly understood physical processes unfold in the system during expansion: the degeneracy of the electrons is lifted, the electron energy spectrum is radically restructured, the dense plasma undergoes partial recombination, a "metal-dielectric" transition occurs in the disordered electronic structure, and a plasma that is nonideal with respect to various types of interparticle interaction is formed.

The experiments of Refs. 121–125 indicates no noticeable discontinuities of the thermodynamic functions and no hydrodynamic anomalies that might be interpreted as specific plasma phase transitions. We stress that the phase transitions discussed in Refs. 1, 2, 79, 80 are most probable precisely in the parameter range studied, since increasing the temperature and lowering the density of a Boltzmann plasma or increasing the pressure of a degenerate plasma results in a relative decrease of the nonideality effects (See Sec. 1).

The highest stages in expansion of the metals in Refs. 121–125 correspond to realization of near-critical states. Entry of the isentropes into the two-phase liquid-vapor region is accompanied by vaporization when it occurs from the liquid-phase side and by condensation when it occurs from the gaseous phase, so

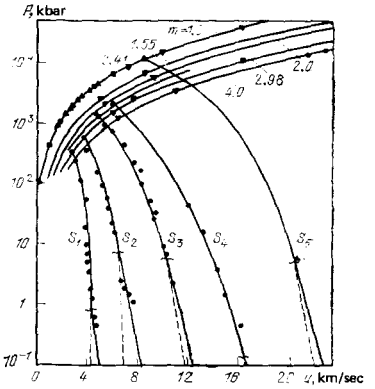

FIG. 24. P–u diagram of copper.[125] Symbols as in Fig. 23.

that the slopes of the isentropes change[137] and the velocity of the decompression wave acquires an additional increment. The presence of these inflections on the experimental curves and their agreement with *a priori* estimates of the vaporization effects[118,129] is additional evidence of the equilibrium nature of the two-phase expansion process. The nature of the thermodynamic information obtained is also in agreement with estimates of the parameters of the critical point and the boiling phase boundary obtained in Refs. 118, 128. It follows from the experiments that the phase diagrams of copper and lead have the usual form in the regions studied, with a single critical point for the "liquid-vapor" phase transition.

Experimental data on isentropic expansion provided a basis for derivation of semiempirical equations of state[138] that describe the existing aggregate of statistical and dynamic data in the solid, liquid and plasma phases, which reproduce melting and vaporization effects, and have the correct asymptotic transition at superhigh pressures and temperatures to the Thomas-Fermi and Debye-Hückel theories. The phase diagram constructed for copper on the basis of such an equation of state[125] appears in Fig. 25.

7. PLASMA PHASE TRANSITIONS

Model theories[1,2,12,188,189] based on physical simplifications and extrapolations of concepts of the quantum and collective effects in Coulomb interaction that have been developed for the weakly nonideal plasma have recently come into extensive use in qualitative analysis of the plasma with strong interparticle interaction because of the serious difficulties encountered in consistent theoretical descriptions of that medium. Characteristically, the system loses thermodynamic stability at high nonidealities in several of these models, a property related[2,5,14,79,80,188,197] to the possibility of a phase transition and separation of the system into phases of unequal density.

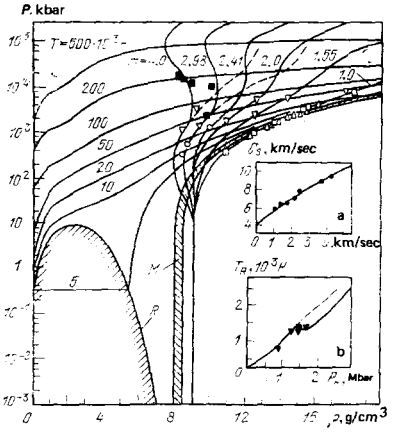

FIG. 25. Phase diagram of copper. The semiempirical equation of state from Ref. 125 was used. m—shock adiabatics for various porosities. The dashed curves represent the adiabatics from Ref. 141. T—isotherms; M, R—melting and boiling phase boundaries; the two-phase regions are shaded. a) sonic velocity c_S on shock adiabatic; b) temperature in decompression wave.[133]

Model analysis of strongly compressed degenerate electron systems[2,12] indicates the possibility of a phase transition with formation of an organized electron structure[147]—the "Wigner crystal." The properties of this crystal and its phase diagram have been investigated in detail in numerous studies (see Refs. 2, 12, 197, 198, 199 and the references therein) in which situations with zero and nonzero temperatures have been considered. In the latter case, the curve separating the electron liquid and the Wigner crystal has a critical point, and the stability limit of this crystal at $T=0$ is quite indefinite ($r_s \gtrsim 33$).[148,200,201] Calculations made by a molecular-dynamics method for the classical single-component plasma[149,202] also predict the formation of a crystal at $\Gamma \sim 155 \pm 10$, which comes close to earlier estimates.[150] These phase transitions were linked to melting of metals in Ref. 151. The dielectric permittivities of strongly compressed Coulomb systems and the stability of the nonideal plasma have been analyzed in thoroughgoing reviews.[203-204]

The situation in the real multicomponent plasma is more complex and varied. Considering polarization to be the basic effect in dense plasma, Mott[152] considered a model in which the intraatomic electrons are in a screened potential $V(r) = -(e^2/r)\exp(r/r_0)$. Numerical solution of the Schrödinger equation for this potential yields the critical value[152] $r_0 \sim 0.84a_0 = 0.84\hbar^2/me^2$, at which the ground state vanishes and which corresponds to the "Mott" metal-dielectric transition.

Possible anomalies in the thermodynamic functions during metallization of dense vapors were discussed by Landau and Zel'dovich,[79] who suggested that metallic systems may contain two phase boundaries: one for the liquid-gas transition and one for the metal-dielectric transition (Fig. 26). The relation of these transitions to plasma anomalies was analyzed in Refs. 80, 153, 189.

A rather large number of recent studies has been devoted to phase transitions in nondegenerate strongly nonideal plasma, using simple models[2,80,12,14,188,154] to analyze the numerous possibilities that appear here. The basic effect responsible for condensation of a multicomponent plasma is the Coulomb attraction between unlike charges, while stabilization of the resulting phase is brought about by quantum effects—interference and, at higher densities, degeneration and overlapping of the electron shells of ions. Phase-transition possibilities in the weakly ionized plasma that arise from the strong charge-neutral interaction have also been discussed.[154] An attempt to move beyond heuristic models was made in Ref. 14, where Monte-Carlo calculations

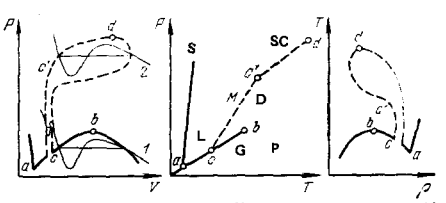

FIG. 26. Schematic diagrams representing possible nature of equilibria in plasma.[79,80,188] a, b) Triple and critical points; *M*) metal; *D*) dielectric.

in a pseudopotential approximation also predicted phase separation of dense plasma.

As gross approximations, the model theories produce highly uncertain predictions, in some cases indicating qualitatively different conclusions, but they are a constant stimulus to experimental searches for these exotic effects.

Possible hydrodynamic effects accompanying dynamic modification of plasma were analyzed in Refs. 137 and 24, which indicate types of phase transitions that can be registered on a shockwise or isentropic change in pressure. Generally, phase anomalies on compression or expansion of metals[34,35,120-125] would be manifested in inflections of the isentropes in Figs. 13, 23, or 24. Especially instructive in this respect are the experiments of Refs. 121–125 (see Figs. 23 and 24), in which it was possible in a single series of experiments to follow the behavior of matter over an extremely broad parameter range and where we might expect most of the phase anomalies predicted by the theory. Results of experiments with isentropic compression[34,35] and expansion of metals[120-125,130,131] and experiments with fast[155] and slow[25] electroexplosion of metals by electric current do not definitely indicate any anomalies caused by phase transitions in nonideal plasma. We note in this context that it is possible in dynamic experiments to record not only vaporization (see Figs. 19, 21, 23), but also an effect with as little influence on flow hydrodynamics[137,24] as melting of matter (see Fig. 21).

Rusakov *et al.*[128] reported studies of the dynamics of dispersal of shock-compressed substances in long (60–200 mm) cylindrical and conical channels. Measuring the velocities of luminous plasmoids and determining the departures of these velocities from self-preserving solutions[156] (obtained for an ideal gas, $\gamma = 1.4$, assuming steadiness of the incident wave), Rusakov *et al.*[178] conclude the phase anomalies occur in the expanding plasma.

Unfortunately, Rusakov *et al.*[178] did not directly register the parameters of the moving plasma in the complex and definitely nonsteady flow, and were therefore obliged to resort to qualitative estimates.

In shock compression of nonideal plasma, phase transitions might change the shock compressibility, an increase of which could, with additional conditions,[137] result in formation of continuous compression wave and multiwave structures, whereas a sharp compressibility decrease could cause the shock wave to lose stability. No anomalies of this kind were detected in experiments with shock compression of cesium and heavy inert gases, and the recorded Hugoniot and Poisson adiabatics (Figs. 10, 11, 13, 23, 24) are smooth curves.

Further, the manner in which the thermodynamic functions of the nonideal plasma were found to vary in experiments (Sec. 5) is consistent with a single-phase situation.

Other evidence indicating that noticeable phase transitions occur in the range of parameters studied is found in the results of electrophysical (Fig. 16) and optical (Fig. 18) measurements, which are interpreted (Sec. 5)

within the framework of single-phase plasma models.

We note that, according to existing conceptions,[23,24,192] phase transitions may take place during very short times ($\sim 10^{-10}$–10^{-6} sec) in dynamic experiments—times much shorter than under static conditions. This makes "tempering" of plasma phases during nonsteady disturbances improbable (though not totally impossible).

In speaking of plasma condensation, it is now the custom[2,5] to appeal to a series of studies[157,158] whose authors claim to have detected anomalous effects at emergence of a detonation wave from a condensed explosive at the free surface of the charge. High-speed motion-picture photography of this process showed with good reproducibility the formation of a brightly luminous plasmoid (see the cover of the journal of Ref. 158), which existed for several tens of microseconds and exhibited electrical conductivity of a "metallic nature."[157,158] The plasmoid changed little in shape during its time of flight and "flowed" along curved glass tubes without causing any visible damage to them, an effect attributed in Refs. 157, 158 to "stability" of the plasma generated, i.e., to the existence of a bonding energy and an internal pressure in the system, as occurs in the Wigner[147] quasicrystalline model of the electronic plasma or in the Ekker-Weizel model of the nondegenerate dense plasma.[159]

According to the interpretation given in Refs. 157, 158 for the observed effects, a "Wigner crystal" forms as a result of "chemical ionization" in the deformation-wave front, and is in a metastable state after this wave emerges from the explosive charge. These plasma concepts were then used as a basis[160] for a model of the detonation of condensed explosives in which the process controlling the detonation is not the shock wave, but electronic heat conduction.

Careful analysis of Refs. 157, 158 showed[161,162] that their interpretation is not the only possible one and can be objected to, and that the conclusions as to the plasma phase transition were not adequately validated, the more so since no direct measurements of density, which would have been affected first by such a transition were made in Refs. 157, 158.

Transillumination of plasma by pulsed x-radiation with wavelengths of 10^{-2} and 0.9 Å indicated[161] the absence of anomalously high plasma densities, while the measured density values were found to be 8–10 times higher than the density of air at atmospheric pressure, in good agreement with the results of the traditional calculation of plasma states behind the front of an air shock wave.[77] Registration of the optical emission from plasma has shown[161,67] that, contrary to the conclusions of Refs. 157, 158, this emission is not anomalous and corresponds to a brightness temperature of $(8-10)\cdot 10^3$ K, which agrees closely with the conventional calculation,[77] and that the optical absorption coefficient of the plasma does not present any anomalies either.[67] The plasmoid electrical conductivity measured in Ref. 64 (Fig. 16) can be described in its entirety by a rarefied-plasma model (Sec. 5). Experiments in which detonation waves escaped into vacuum[161] and helium[162] indicated no emission of light by the plasma, although according to the conception of Refs. 157, 158 this emission should, if anything, have been stronger. Rather artificial arguments involving a "reaction thrust on recombination" were used to explain the observed plasmoid velocities in Ref. 157, 158, although these velocities can be calculated easily on the basis of the decay of the discontinuity at the explosive-air interface. Thus, the experiments of Refs. 161 and 162 and analysis of available data indicate that the thermodynamic, optical, electrophysical, hydrodynamic, and mechanical properties of the plasmoid are fully described by an ideal-plasma model on the assumption that this plasmoid is formed by compression and irreversible heating of air in the front of the wave formed on expansion of the detonation products of the condensed explosive. The basic reason for the incorrect inference of plasma condensation in Refs. 157, 158 was the low speed of lateral expansion of the glass tube walls owing to their considerable mass, an effect that was erroneously interpreted as "stability" of the plasma.

Electronic phase transitions associated with transfer of inner electron shells of an atom or ion from the discrete to the continuous spectrum may appear in a strongly compressed plasma. Phase transitions associated with redistribution of electrons among shells during compression were analyzed theoretically by band-theory methods in Refs. 163, 164 and were registered experimentally in Refs. 165, 23. References 11 and 166 predict electron transformations in the ultramegabar pressure range that correspond to first-order phase transitions, with a given electron shell in the continuous spectrum in one phase and in the discrete spectrum in the other. Naturally, such electron transitions correspond essentially to a series of phase transitions caused by "pressure ionization" of a sequence of electron shells. Estimation of the parameters of these transformations by the methods of the quasiclassical theory[166] gives pressures higher than 300 Mbar, the prospects for attainment of which will be discussed in the next section.

8. GENERATION OF SUPERDENSE PLASMA IN SHOCK WAVES

According to present conceptions,[1,11] the properties of plasma become radically simpler at extremely high pressures and densities, when the inner electron shells of atoms and ions are "crushed" and electron density is distributed in quasiuniform fashion within elementary Wigner-Seitz cells. The quasiclassical approximation to the self-consistent-field method,[11] in which the description is given not in the quantum-mechanical language of wave functions and eigenvalues, but in terms of the average density of the electron component of the plasma, is valid in this case. These conceptions form the basis of the Thomas-Fermi model, whose range of validity is determined by the smallness of volume, correlation, and shell effects.[11] The corresponding letter criteria of their smallness give $P_{\lim} \gg e^2/a_0^4$ as a general estimate of the lower limit of validity of the Thomas-Fermi model, a figure that corresponds to extremely high pressures $\gg 300$ Mbar

($T=0$), which greatly exceed the capabilities of experimental arrangements based on the use of chemical condensed explosives.[20-24] Therefore an active search is now in progress for alternative methods of generating ultrahigh parameters that would enable us to approach the region of the quasiclassical description with the object of estimating its true limit of validity. These methods include the use of powerful shock waves formed in the near zones of strong explosions,[6,27-30,32,177,180,221] the use of coherent laser radiation,[167-172,219] relativistic electron and ion beams,[211,214] electrodynamic acceleration methods,[215-218] and electrical explosion of thin metal foils.[173-174]

In experiments with strong shock waves[6,27-30,32,177,180,221] made by the reflection procedure, the dynamic compressibilities of the substances were determined at pressures in the tens and hundreds of megabars by a comparative method: by recording the velocities of shock waves passing through successive layers of test substances, one of which was a standard. Standards used in experiments with dynamic compression of compact substances were lead[27-29] and iron,[32] for which interpolated shock adiabatics were plotted to connect the range of superhigh ($P \gtrsim 100$ Mbar) pressures to the $\lesssim 10$ Mbar pressures accessible to direct[20,23] experiments.

Extrapolation of the experimental data of Ref. 28 to high pressures gave an estimate of ~150 Mbar for the lower limit of validity of the Thomas-Fermi theory. The reworking of these data undertaken in Ref. 31, using an improved variant of the standard shock adiabatic of lead (quantum exchange and correlation corrections were applied[11]) led to the conclusion that the quantum-statistical models are valid beginning at pressures of ~300 Mbar for cold matter and at 50 Mbar for T = 10 eV.

However, this conclusion is contradicted by later experiments[32,180] (Fig. 27) in which strong deviations from the Thomas-Fermi model were registered on Pb, Fe, Al, and SiO_2 at pressures of 10–160 Mbar. According to Refs. 32, 180, these differences result from so-called "oscillation effects"[166] that are governed by the discrete energy spectrum and which lead to sharply nonmonotonic behavior of the thermodynamic functions, and are not taken into account by the elementary models.[175] The presence of oscillations caused by the shell structure at superhigh ($P \gtrsim 300$ Mbar) pressures also follows from more accurate calculations made by the associated plane-wave method[126] and from other quantum-mechanical models.[113,181] Therefore the question of methods for theoretical description of the superdense plasma and specifically the question of the actual limit of validity of the quasiclassical methods remains open and is an object of increased interest.

Figure 28 shows results of experiments in the compression of porous copper by strong shock waves[30] that produce extremely high heat-energy concentrations. A superdense quintuply ionized weakly degenerate ($n\lambda$ ~0.7) plasma with extremely high parameters: P ~20.9 Mbar, $n_e \sim 2 \cdot 10^{23}$ cm^{-3}, $\Gamma \sim 2$ is formed at the maximum temperatures of $\sim 2.5 \cdot 10^5$ K. Figure 28 illustrates a reasonable description of the properties of this medium by the "bounded atom" plasma model[73,78] with short-range repulsion taken into account within the framework of a hard-sphere model (see, further, Ref. 240). The errors that arise in the description of the properties of dense plasma with the Thomas-Fermi model are discussed in Ref. 220.

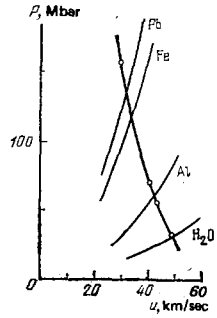

FIG. 27. Parameters of shock compression in experiment of Ref. 32. The curves were calculated after Ref. 31.

Experiments in which comparative compressibilities were registered[27-30,32,177] are subject to an uncertainty related to the extrapolation procedure used in plotting the shock adiabatic of the reference standard. There is no such uncertainty in experiments with absolute registration of states on the shock adiabatics of molybdenum[6] and aluminum[180] at superhigh pressures. In the experiments of Ref. 6, a block of uranium-235 was placed 1.1 m from a nuclear charge (Fig. 29) behind a B_4C slow-neutron absorber, and a molybdenum test specimen with internal lightguides for baseline registration of the velocity of the shock-wave front was mounted on the block. The neutron flux formed on detonation of the nuclear device A causes rapid volume heating of the uranium to a temperature of ~50 eV, which, on subsequent expansion of the uranium, results in the generation of a plane shock wave with an amplitude pressure of ~20 Mbar in the molybdenum. Measurement of a second kinematic parameter—the velocity of motion of the shock-compressed molybdenum—was based on the Doppler shift of the resonant neutron-absorption lines at energies of 0.3–0.8 keV, which were

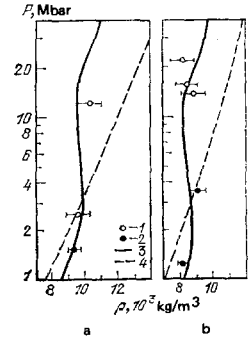

FIG. 28. Compression of porous copper by shock waves. a) initial porosity $m = \rho_0/\rho_{00} = 3$; b) $m = 4$. The circles represent experiments. 1) Ref. 30; 2) Ref. 141. The solid curves (3) are the shock adiabatics calculated from the chemical plasma model[1] (5.1)–(5.5). The dashed lines (4) represent the Thomas-Fermi theory with corrections (Ref. 175).

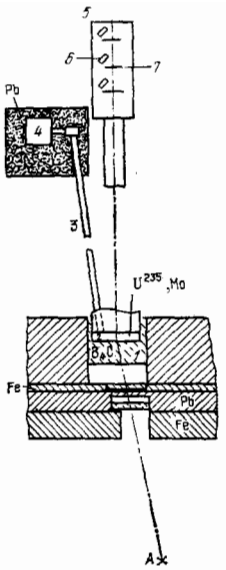

FIG. 29. Diagram of experiments to generate strong shock waves by nuclear detonation.[6] A) Nuclear charge; 1) B_4C slow-neutron absorber; 2) test assembly of uranium 235 and molybdenum; 3) lightguides (length 12 m); 4) optical radiation recorders; 5) time-of-flight neutron spectrometer; 6) solid-state detectors; 7) lithium and plutonium foils.

registered with a time-of-flight neutron spectrometer. Molybdenum was later[177] used as a standard in experiments to measure the comparative compressibilities of uranium at pressures of ~67 Mbar (which gave pressures higher than those predicted by the quasiclassical theory) and those of 13 other substances at pressures of 10 to 70 Mbar.[221] We note that it was found necessary in reducing these data[177] to resort to extrapolation (from $P \sim 20$ Mbar to $P \sim 50$ Mbar) of the reference molybdenum adiabatic. In the absolute measurements of Ref. 180, the phase and mass velocities of shock waves in aluminum were registered with γ-active reference layers and slit collimators placed parallel to one another, the distance between them forming the measurement base. The γ-radiation registered by the scintillation sensors was formed as a result of neutron absorption by reference specimens inserted into the aluminum, which were made from a material with a large radiative capture cross section (europium). The results of these experiments indicate (Fig. 30) significant differences (of up to a factor of 3 in the pressure) between the quantum-statistical model at $P \sim 11$ Mbar and experiment, although it is difficult to form a judgement as to the actual error of the measurements on the basis of the data reported in Ref. 180.

Lasers offer a unique opportunity for focusing of coherent electromagnetic radiation onto small ($\sim 10^{-4}$ cm^{-2}) surfaces, which results in extremely high local energy concentrations.[8,219] Specific intarget powers $W \sim 10^{14}$–10^{17} W/cm^2 are presently attainable, and it appears that the limit may be raised to 10^{20} W/cm^2 in the very near future.[169] The "recoil pulse" that appears under the action of these light fluxes generates a strong shock wave that can be used for compression and irreversible heating of the dense plasma of the targets investi-

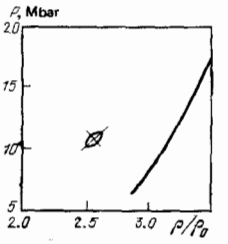

FIG. 30. Comparison of data from absolute measurements of shock compressibility of aluminum[180] with results of interpolation[31] based on quantum-statistical model.

gated.[167,169,171,172] Analysis[169] of hydrodynamic intensity calculations made for shock waves formed when existing and planned laser systems are turned onto various materials indicates (Fig. 31) that we have a real opportunity for advancing into the ultramegabar pressure range and investigating the properties of superdense plasma.

A number of specific requirements[169,172,219,227] dictated by the physical peculiarities of the process and by the characteristics of the diagnostic tools must be met in the design of laser targets for such experiments. The thickness of the target is determined by the need to eliminate distorting decompression waves at the end of the laser pulse and to minimize the influence of "nonthermal" electrons that appear in the resonant absorption band of the laser radiation. The diameter of the target is specified[169] to obtain a high intensity of the radiation and eliminate side decompression waves. In addition, the target must be small enough,[170,169] or else special screens must be used,[226,225] to diminish the role of surface currents from the heated plasma.

The first experiments with generation of shock waves in hydrogen and Plexiglas were made with a low-power neodymium laser[167] with an energy $q \sim 12$ J and a pulse

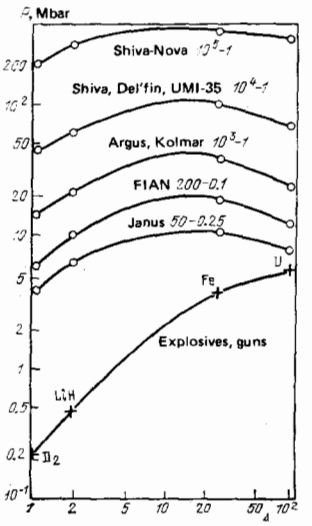

FIG. 31. Maximum amplitudes of shock waves[169] generated by various laser systems. The first figure is the energy in joules, the second the flash time in units of 10^{-9} sec; the lower curve indicates the parameters accessible to chemical-explosive and light-gas-gun techniques; A is the atomic number of the target element.

duration $\tau \sim 5 \cdot 10^{-9}$ sec. Because of the small size of focal spot (40 μm), the shock waves damped rapidly and degenerated into spherical waves. A more powerful laser system, $q \sim 30$ J, $\tau \sim 0.3 \cdot 10^{-9}$ sec, was used in Ref. 171 to produce plane shock waves. Varying the time of passage of the shock wave through a stepped aluminum specimen made it possible to register a shock-wave front velocity of 13 km/sec, which corresponds to a pressure of ~2 Mbar. These pressures were increased[172] by an order of magnitude (Fig. 32) by using a laser with higher parameters, $q \sim 100$ J, $\tau \sim 0.3 \cdot 10^{-9}$ sec, which gave radiation intensities of $8 \cdot 10^{13}$–$3 \cdot 10^{14}$ W/cm^2 at the target. In this case[172] a small-diameter target was used, since the authors felt that it would diminish the importance of surface currents,[170] and the results agreed with theory. At this time, the highest pressures, $P \sim 35$ Mbar, have been obtained[222] on the "Shiva" laser installation[222] by illuminating a composite aluminum-and-gold target with a light flux of $W \sim 3 \cdot 10^{15}$ W/cm^2. A "reflection" method[20] in which a shock wave crossed from aluminum ($P \sim 3$ Mbar) into gold ($P \sim 6$ Mbar) was used in the experiments of Ref. 224 to obtain information on the mass velocity of plasma motion. Use of a CO_2 laser[225] under the conditions of $W \sim 4.5 \cdot 10^{13}$ W/cm^2, at which nonthermal electrons are unimportant, produced a shock-wave intensity of ~5 Mbar in aluminum.

Analysis of physical processes in the laser plasma indicates[227, 219] that the main limitation on generation of shock waves in homogeneous targets is heating of the material by high-energy electrons that appear in the resonant absorption band. Therefore the use of short-wave laser radiation (obtained using nonlinear KDP crystals or in KrF, Se, or other systems) makes it possible to broaden the range of attainable pressures significantly. Impingement of thin foils that have been accelerated to velocities in the tens of km/sec by laser radiation is another promising method of generating superdense plasma.[228, 229]

An interesting example of the use of nonthermal electrons for isochoric plasma heating was reported in Ref. 226, where nonthermal electrons with $T_e \sim 15$ keV caused rapid heating and explosion of a three-micron layer of aluminum, which, as it expanded, generated a shock wave with an amplitude pressure of ~13 Mbar.

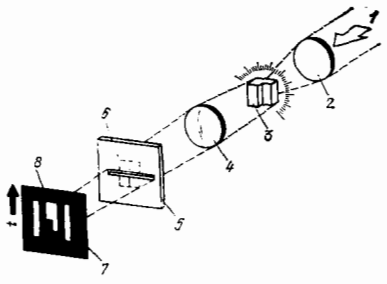

FIG. 32. Diagram of experiment in laser generation of shock waves.[171, 172] 1) Laser radiation, 2) focusing system; 3) stepped target; 4) image-converter optics; 5) image-converter slit; 6) image of target; 7) photographic film; 8) recorded image.

Experiments with laser systems make extremely high demands on diagnostic apparatus. The temporal and spatial resolutions must be no worse than 10^{-11} sec and 10^{-4} cm. As result, it is possible in most contemporary laser experiments[167, 171, 172, 222, 224, 225, 226] to measure only the velocity of the shock wave, while a wide variety of possibilities: the obstacle method,[224, 232] flash radiography,[230] the Doppler line shift,[169] and others have been considered for registration of another dynamic parameter—the velocity of plasma motion.

The powerful (~10^{14} W) pulsed relativistic-electron and -ion generators that have been developed for controlled thermonuclear fusion and solution of applied problems[211-214] are capable of focusing high-intensity beams on targets a few millimeters in diameter. The specific powers of ~10^{14}–10^{18} W/cm^2 put into the target in this way cause vaporization and dispersal of its outer part and generation of strong shock waves by ablation.

Applying the same requirements as in the case of laser action[227, 219] to the one-dimensionality and quasisteadiness of the plasma flow in the target and remembering that the characteristic free paths of electrons with ~MeV energies in metals are ~0.1–1 mm, we can estimate the amplitudes of shock waves in plasma at the decamegabar level.[232] The maximum pressures do not exceed ~3 Mbar in the first experiments now being performed in the generation of shock waves in metals with relativistic electron beams.[212, 213, 233] The velocities of motion and the time profiles of the shock waves, which give information on the strength properties of the materials and the parameters of the equation of state, have been recorded. Ablation acceleration of foils under the action of x-rays, which occurs on deceleration of a relativistic electron beam in the outer metallic part of a target,[234] offers interesting possibilities. A polyethylene envelope was accelerated in this way to ~$5 \cdot 10^6$ cm/sec in a conical target, and a D-D reaction neutron yield of ~$3 \cdot 10^6$ neutrons per pulse has been registered.

A scheme that uses impingement of macroscopic liners (mass ~0.1 g) accelerated to velocities of 10^7–10^8 cm/sec[215, 218] is attracting steadily increasing attention along with the now traditional methods of pulsed controlled thermonuclear fusion excited by laser radiation or by charged-particle fluxes. It is evident that the high-velocity propulsion devices based on electrodynamic acceleration methods that are considered for these purposes can be used to generate ultrastrong shock waves and with their aid to investigate the properties of plasma at extreme pressures and temperatures. In a linear magnetodynamic accelerator, a superconductive striker is accelerated in an inhomogeneous magnetic field created by coils that are switched on in synchronism with the motion of the striker.[235] In the design of Ref. 236, the striker is accelerated by a series of Z pinches that collapse toward the axis of symmetry.

The railgun accelerator[215-217] is currently farthest advanced among the many electrodynamic accelerators for solids. In this device (Fig. 33), the striker 1 is accelerated under the action of a ponderomotive force

$$F = \frac{1}{2} J^2 L$$

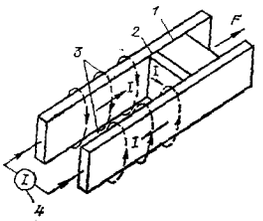

FIG. 33. Diagram of railgun.[216] 1) striker; 2) electric arc; 3) current-conducting rails; 4) power source.

on passage of an electric current J through the electrodes 3 (linear inductance L). The accelerating force F must not exceed the strength limits of the striker material ($J \lesssim 1$ MA[216]), and the best possible electrical contact with the rails is provided by an electric arc 2 that burns at the rear of the dielectric linear and is pressed against it by the magnetic field. The serviceability of such systems was demonstrated in the experiments of Ref. 237, where velocities $W \sim 6$ km/sec ($m \sim 3$ grams) were obtained with a railgun powered by an inductive accumulator and a homopolar generator (energy 500 mJ), and in Ref. 217, where the use of a bank of condensers (energy ~0.6 MJ) and a linear magnetocumulative generator increased the propulsion velocity to 10–11 km/sec.

Still another way to move up the pressure scale is found in the electrical explosion of conductors, which occurs when a powerful condenser bank is discharged across them (Fig. 34). In Refs. 173, 174, 238, a 17.2-MF, 100-kV condenser bank imparts a specific energy 10–100 times larger than the characteristic internal energy of condensed explosives to a thin aluminum foil. As it expands, the foil accelerates a tantalum striker ~13 μm thick to 16 km/sec, which corresponds to an impact pressure of ~20 Mbar. The velocity of the shock-wave front (stepped target) and the flight velocity of the striker (Fabry-Perot laser interferometer) are registered under the conditions of this experiment.[173,174] which, in accordance with the reflection method,[20] may yield quantitative information on the dynamic compressibility of the test material. Methodological experiments[238] to record the shock compressibility of tantalum at pressures up to 4.5 Mbar are currently being conducted on this installation.

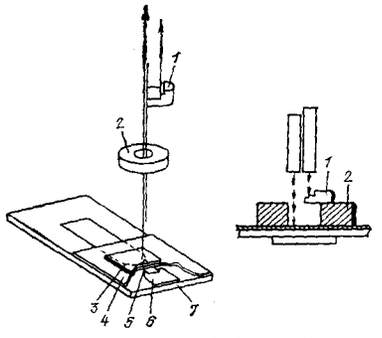

FIG. 34. Diagram of electrodetonation apparatus.[173,174] 1) stepped target; 2) channel for striker motion; 3) projectile plate; 4) plastic insulating spacer; 5) exploding foil; 6) current busbars; 7) massive base.

Thus, the use of new sources of pulsed local energy concentration in dynamic plasma physics will make it possible in the near future to generate shock waves of extreme intensity and to advance into the region of exotically high plasma pressures and temperatures.

The author thanks F. I. Dubovitskiĭ and A. M. Prokhorov (at whose suggestion this review was prepared) for their support of the work, and L. V. Al'tshuler, L. P. Pitaevskiĭ, and B. M. Smirnov for helpful discussions and valuable comments on the manuscript.

[1]V. E. Fortov, Modeli uravneniĭ sostoyaniya veshchestva (Models of the Equations of State of Matter). RIO IKhF Akad. Nauk SSSR, Chernogolovka (1980).
[2]G. É. Norman and A. N. Starostin, Teplofiz. Vys. Temp. **8**, 413 (1970).
[3]V. K. Gryaznov *et al.*, Teplofizicheskie svoĭstva rabochikh sred yadernoĭ énergeticheskoĭ ustanovki s gazofaznym reaktorom (Thermo-physical Properties of Working Fluids for the Gaseous-Phase-Reactor Nuclear Powerplant), Atomizdat, Moscow (1980).
[4]Research on Uranium Plasmas and Their Technological Applications: Proc. of Symposium in Gainessville, Florida/ Ed. K. Thom, R. T. Schneider, Washington: NASA, 1971; 2-nd Symposium on Uranium Plasmas. Atlanta, Georgia (1971).
[5]L. S. Polak (ed.), Ocherki fiziki i khimii nizkotemperaturnoĭ plazmy (Outlines in the Physics and Chemistry of the Low-Temperature Plasma) Nauka, Moscow (1971).
[6]C. E. Ragan III, M. G. Silbert, and B. C. Diven, J. Appl. Phys. **48**, 2800 (1977); in: High Pressure Science and Technology/Ed. B. Vodar, Ph. Marteau.—Pergamon Press, London; 1980, v. 2, p. 993.
[7]J. G. Linhart, Nucl. Fusion **10**, 211 (1970).
[8]P. Caldirola and M. Knoepfel (eds.), The Physics of High Energy Density, Academic Press (1971) [Russ. Transl., Mir, Moscow, 1974].
[9]Jupiter I and II. Russian translation edited by V. N. Zharkov. Mir, Moscow (1978).
[10]A. M. Prokhorov, S. I. Anisimov, and P. P. Pashinin, Usp. Fiz. Nauk **119**, 401 (1976) [Sov. Phys. Usp. **19**, 547 (1976)].
[11]D. A. Kirzhnits, Yu. E. Lozovik, and G. V. Shpatakovskaya, *ibid.* **117**, 3 (1975) [**18**, 649 (1976)].
[12]W. Ebeling, W. Kraft, and D. Kremp, Theory of Bound States and Ionization Equilibrium in Plasmas and Solids [Russ. Transl., Mir, Moscow (1979)].
[13]L. P. Kudrin, Statisticheskaya fizika plazmy (Statistical Plasma Physics), Atomizdat, Moscow (1974).
[14]V. M. Zamalin, G. É. Norman, and V. S. Filinov, Metod Monte-Karlo v statisticheskoĭ termodinamike (The Monte Carlo Method in Statistical Thermodynamics). Nauka, Moscow (1977).
[15]R. Balescu, Statistical Mechanics of Charged Particles, Wiley, 1963 [Russ. Transl., Mir, Moscow (1967)].
[16]P. P. Kulik, G. E. Norman, and L. S. Polak, Khim. vys. énergiĭ **10**, 203 (1976); **11**, 195 (1977).
[17]V. A. Alekseev, Teplofiz. Vys. Temp. **8**, 641 (1970); Usp. Fiz. Nauk **106**, 393 (1972) [Sov. Phys. Usp. **15**, 139 (1972)].
[18]É. I. Asinovskiĭ and V. A. Zeĭgarnik, Teplofiz. Vys. Temp. **12**, 1278 (1974).
[19]R. G. Ross and D. A. Greenwood, Prog. Mater. Sci. **14**, 173 (1971).
[20]L. V. Al'tshuler, Usp. Fiz. Nauk **85**, 197 (1965) [Sov. Phys. Usp. **8**, 52 (1965)].
[21]S. B. Kormer, *ibid.* **94**, 641 (1968) [**11**, 229 (1968)].
[22]V. N. Mineev and A. G. Ivanov, *ibid.* **119**, 75 (1976) [**19**, 400 (1976)].

[23]L. Davison and R. A. Graham, Phys. Rept. **55**, 256 (1979).
[24]G. E. Duvall and R. A. Graham, Rev. Mod. Phys. **49**, 525 (1977).
[25]J. W. Shaner and G. R. Gathers, In: High Pressure Science and Technology/Ed. Timmerhous and M. S. Barber, N.Y.: Plenum, Press, 1979. V. 12, p. 847.
[26]Ya. B. Zel'dovich and Yu. P. Raĭzer, Fizika udarnykh voln i vysokotemperaturnykh gidrodinamicheskikh yavleniĭ (Physics of Shock Waves and High-Temperature Hydrodynamic Phenomena), Nauka, Moscow (1966).
[27]L. V. Al'tshuler, B. N. Moiseev, L. V. Popov, G. V. Simakov, and R. F. Trunin, Zh. Eksp. Teor. Fiz. **54**, 785 (1968) [Sov. Phys. JETP **27**, 420 (1968)].
[28]R. F. Trunin, M. A. Podurets, G. V. Simakov, L. V. Popov, and B. N. Moiseev, *ibid.* **60**, 1044 (1972) [**33**, 567 (1971)].
[29]R. F. Trunin, M. A. Podurets, B. N. Moiseev, G. V. Simakov, and L. V. Popov, *ibid.* **56**, 1172 (1969) [**29**, 630 (1969)]; Izv. Akad. Nauk SSSR. Ser. Fizika Zemly No. 1, 13 (1971).
[30]V. N. Zubarev, M. A. Podurets, L. V. Popov, G. V. Simakov, and R. F. Trunin, in: Detonatsiya (Detonation), OIKhF Akad. Nauk SSSR. Chernogolovka, 1978, p. 61.
[31]L. V. Al'tshuler, N. N. Kalitkin, L. V. Kuz'mina, and B. S. Chekin, Zh. Eksp. Teor. Fiz. **76**, 1212 (1979) [Sov. Phys. JETP **49**, 615 (1979)].
[32]L. P. Volkov, N. P. Voloshin, R. A. Mangasarov, V. A. Simonenko, G. V. Sin'ko, and V. L. Sorokin, Pis'ma Zh. Eksp. Teor. Fiz. **31**, 546 (1980) [JETP Lett. **31**, 513 (1980)]; E. N. Avrorin, B. K. Vodolaga, L. P. Volkov, A. S. Vladimirov, V. A. Simomenko, and B. T. Chernovolyuk, *ibid.* 727 [685].
[33]B. N. Lomakin and V. E. Fortov, Zh. Eksp. Teor. Fiz. **63**, 92 (1972) [Sov. Phys. JETP **36**, 48 (1973)].
[34]A. G. Kunavin, A. V. Kirillin, and Yu. S. Korshunov, Teplofiz. Vys. Temp. **11**, 261 (1973); **13**, 1304 (1974).
[35]I. M. Isakov, and B. N. Lomakin, Teplofiz. Vys. Temp. **17**, 262 (1979).
[36]P. S. Lusne and D. R. Hardesty, J. Chem. Phys. **59**, 6513 (1973); V. E. Fortov, Fiz. gor. i vzryva, **8**, 428 (1972).
[37]S. B. Kormer, A. I. Funtikov, V. D. Urlin, and A. N. Kolesnikova, Zh. Eksp. Teor. Fiz. **42**, 686 (1962) [Sov. Phys. JETP **15**, 477 (1962)].
[38]V. E. Fortov and Yu. G. Krasnikov, *ibid.* **59**, 1645 (1970) [**32**, 897 (1971)].
[39]V. E. Fortov, Zh. Prikl. Mekh. Tekh. Fiz. No. 6 (1972); in: Gorenie i vzryv (Combustion and Explosion), Nauka, Moscow, 1972, p. 56.
[40]A. V. Bushman, B. N. Lomakin, V. A. Sechenov, V. E. Fortov, O. E. Shchekotov, and I. I. Sharipdzhanov, Zh. Eksp. Teor. Fiz. **69**, 1624 (1975) [Sov. Phys. JETP **42**, 828 (1975)].
[41]I. Ya. Dikhter and V. A. Zeĭgarnik, Teplofiz. Vys. Temp. **15**, 471 (1977).
[42]S. G. Barol'skiĭ, N. V. Ermokhin, P. P. Kulik *et al.* Zh. Eksp. Teor. Fiz. **62**, 176 (1972) [Sov. Phys. JETP **35**, 94 (1972)]; Teplofiz. Vys. Temp. **9**, 665 (1971); **15**, 693 (1979).
[43]B. N. Lomakin, V. E. Fortov, and O. E. Shchekotov, Teplofiz. Vys. Temp. **8**, 154 (1970); **9**, 628 (869).
[44]V. A. Sechenov and O. E. Shchekotov, Teplofiz. Vys. Temp. **12**, 652 (1974).
[45]B. N. Lomakin and V. E. Fortov, Teplofiz. Vys. Temp. **9**, 66 (1971).
[46]K. I. Seryakov, Fiz. Gor. i Vzryva, No. 1, 48 (1970).
[47]V. A. Sechenov, É. A. Son, and O. E. Shchekotov, Pis'ma Zh. Tekh. Fiz. **1**(10), 891 (1975) [Sov. Tech. Fiz. Lett. **1**, 388 (1975)]; Teplofiz. Vys. Temp. **15**, 411 (1977).
[48]G. A. Pavlov and V. M. Kucherenko, *ibid.* 409.
[49]Yu. N. Ryabinin, Gazy pri bol'shikh plotnostyakh i vysokikh temperaturakh (Gases at High Densities and Temperatures), Fizmatgiz, Moscow (1959).
[50]V. A. Volkov, A. B. Karasev, and B. K. Tkachenko, Acta Astronautica **14**, 371 (1976); Teplofiz. Vys. Temp. **16**, 411 (1978); Fiz. Plazmy **6**, 1115 (1980) [Sov. J. Plasma Phys. **6**, 613 (1980)].
[51]B. K. Tkachenko, S. I. Titarov, A. B. Karasev, and S. V. Alipov, Fiz. Gor. i Vzryva No. 5, 763 (1976); in: IV Konferentsiya po teplofizicheskim svoĭstvam veshchestv. Tezisy (Fourth Conference on the Thermophysical Properties of Matter. Abstracts), Minsk, 1978; in: VI Konferentsiya po dinamike izluchayushchego gaza. Tezisy (Sixth Conference on the Dynamics of Radiatins Gases. Abstracts), Moscow (1980).
[52]R. H. Christian and F. L. Yarder, J. Chem. Phys. **33**, 2042 (1955).
[53]W. E. Deal, J. Appl. Phys. **28**, 782 (1957).
[54]Explosives Research Laboratory. Bruceton, Pa. OSRD, 1943. 1488.
[55]M. A. Tsikulin and E. G. Popov, Izluchatel'nye svoĭstva udarnykh voln v gazakh (Emissive Properties of Shock Waves in Gases), Nauka, Moscow (1977).
[56]I. F. Zharkov, I. V. Nemchinov, and M. A. Tsikulin, Zh. Prikl. Mekh. Tekh. Fiz. No. 1, 31 (1967).
[57]A. N. Dremin and S. D. Savrov, Dokl. Akad. Nauk SSSR **179**, 624 (1968).
[58]E. G. Popov, A. A. Provalov, and M. A. Tsikulin, *ibid.* **194**, 805 (1970) [**15**, 933 (1971)].
[59]H. Petschek *et al.*, J. Appl. Phys. **26**, 83 (1955).
[60]V. K. Gryaznov, I. L. Iosilevskiĭ, and V. E. Fortov, Zh. Prikl. Mekh. Tekh. Fiz. No. 3, 70 (1973).
[61]E. I. Zababakhin, in: Mekhanika v SSSR za 50 let (50 years of Mechanics in the USSR), Nauka, Moscow, 1970, p. 313.
[62]V. E. Fortov, Yu. V. Ivanov, A. N. Dremin, V. K. Gryaznov, and V. E. Bespalov, Dokl. Akad. Nauk SSSR **221**, 1307 (1975) [Sov. Phys. Dokl. **20**, 295 (1975)]; Zh. Eksp. Teor. Fiz. **69**, 1624 (1975) [Sov. Phys. JETP **42**, 828 (1975)].
[63]V. E. Besplaov, V. K. Gryaznov, A. N. Dremin, and V. E. Fortov, *ibid.* 2059 [1046].
[64]Yu. V. Ivanov, A. N. Dremin, V. B. Mintsev, and V. E. Fortov, Zh. Eksp. Teor. Fiz. **71**, 216 (1976) [Sov. Phys. JETP **44**, 112 (1976)].
[65]B. B. Mintsev and V. E. Fortov, Pis'ma Zh. Eksp. Teor. Fiz. **30**, 401 (1979) [JETP Lett. **30**, 375 (1979)].
[66]I. T. Modell, Zh. Eksp. Teor. Fiz. **32**, 714 (1957) [Sov. Phys. JETP **5**, 589 (1957)].
[67]V. E. Bespalov, L. G. D'yachkov, G. A. Kobzev, and V. E. Fortov, Teplofiz. Vys. Temp. **17**, 266 (1979).
[68]Yu. V. Ivanov, V. B. Mintsev, A. N. Dremin, and V. E. Fortov, Pis'ma Zh. Tekh. Fiz. **2**, 97 (1976) [Sov. Tech. Phys. Lett. **2**, 37 (1976)].
[69]V. B. Mintsev, V. K. Gryaznov, and V. E. Fortov, Zh. Eksp. Teor. Fiz. **79**, 116 (1980) [Sov. Phys. JETP **52**, 59 (1980)].
[70]A. E. Voĭtenko, Dokl. Akad. Nauk SSSR **158**, 1278 (1964); **169**, 547 (1966) [Sov. Phys. Dokl. **11**, 596 (1967)].
[71]V. E. Fortov, A. A. Leont'ev, A. N. Dremin, S. V. Pershin, in: Teplofizicheskie svoĭstva nizkotemperaturnoĭ plazmy (Thermophysical Properties of the Low-Temperature Plasma), Nauka, Moscow, 1975, p. 39.
[72]V. E. Fortov, A. A. Leont'ev, V. K. Gryaznov, and A. N. Dremin, Zh. Eksp. Teor. Fiz. **71**, 225 (1976) [Sov. Phys. JETP **44**, 116 (1976)].
[73]V. K. Gryaznov, M. V. Zhernokletov, V. N. Zubarev, I. L. Iosilevskiĭ, and V. E. Fortov, Zh. Eksp. Teor. Fiz. **78**, 573 (1980) [Sov. Phys. JETP **51**, 288 (1980)].
[74]M. V. Zhernokletov, V. N. Zubarev, and G. S. Telegin, Zh. Prikl. Mekh. Tekh. Fiz. No. 4, 127 (1969).
[75]J. Roth, J. Appl. Phys. **35**, 1429 (1964).
[76]V. E. Bespalov, V. K. Gryaznov, and V. E. Fortov, Zh. Eksp. Teor. Fiz. **76**, 140 (1979) [Sov. Phys. JETP **49**, 71 (1979)].
[77]N. M. Kuznetsov, Termodinamicheskie funktsii i udarnye adiabaty vozdukha pri vysokikh temperaturakh (Thermodynamic Functions and Shock Adiabatics of Air at High Temperatures), Mashinostroenie, Moscow (1965).
[78]V. E. Fortov, V. K. Grasnov, and A. N. Ivanova, In: XIII Intern. Conference on Phenomena in Ionized Gases. Berlin, 1977, p. 218.
[79]L. D. Landau and Ya. B. Zel'dovich, Zh. Eksp. Teor. Fiz.

14, 32 (1944).
[80]G. É. Norman, *ibid.* **60**, 1686 (1971) [Sov. Phys. JETP **33**, 912 (1971)].
[81]B. V. Zelener, Teplofiz. Vys. Temp. **15**, 893 (1977).
[82]E. Mason and T. Spurling, The Virial Equation of State, Pergamon, (1970) [Russ. Transl. Mir, M. (1972)].
[83]H. N. V. Temperley, J. S. Rawlinson, and G. S. Rushbrooke (eds.), Physics of Simple Liquids, North Holland, Amsterdam (1968) [Russ. Transl. Mir, M. (1971)].
[84]V. K. Gryaznov and I. L. Iosilevskiĭ, Chislennye metody mekhaniki sploshnoi sredy (Numerical Methods in the Mechanics of Continuous Media) (Novosibirsk) **4**, No. 5, 166 (1973).
[85]L. Spitzer, Physics of Fully Ionized Gases, Wiley, New York (1962) [Russ. Transl. Mir, M. (1965)].
[86]A. L. Khomkin, Teplofiz. Vys. Temp. **10**, 870 (1974).
[87]Yu. L. Klimontovich and V. Ebeling, Zh. Eksp. Teor. Fiz. **63**, 905 (1972) [Sov. Phys. JETP **36**, 476 (1973)].
[88]H. A. Gould and H. E. DeWitt, Phys. Rev. **155**, 68 (1967); R. H. Williams and H. E. DeWitt, Phys. Fluids, **12**, 2326 (1969).
[89]T. Kihara and O. Aono, J. Phys. Soc. Japan **18**, 837 (1963); I. Itakawa, *ibid.* 1499.
[90]A. A. Valuev and A. L. Norman, Teplofiz. Vys. Temp. **15**, 191 (1977).
[91]V. S. Vorob'ev and A. L. Khomkin, *ibid.* **14**, 204 (1976).
[92]V. K. Gryaznov, Yu. V. Ivanov, A. N. Starostin, and V. E. Fortov, *ibid.* 643.
[93]F. Blatt, Physics of Electronic Conduction in Solids, McGraw-Hill, N.Y., (1968) [Russ. Transl., Mir, M. (1971)].
[94]R. N. Keeler, M. van Thiel, and B. J. Alder, Physica **31**, 1437 (1965).
[95]E. M. Conwell and V. E. Weiscopf, Phys. Rev. **77**, 388 (1950).
[96]B. M. Kovalev, P. P. Kulik, B. N. Lomakin, V. A. Ryabyĭ and V. E. Fortov, Fiz. Gor. i Vzryva, No. 10, 289 (1974).
[97]B. M. Askerov, Kineticheskie éffekty v poluprovodnikakh (Kinetic Effects in Semiconductors), Nauka, Moscow, 1970.
[98]N. V. Ermokhin, B. M. Kovalev, P. P. Kulik, and V. A. Ryabyĭ, Teplofiz. Vys. Temp. **15**, 695 (1977).
[99]N. N. Kalitkin, L. V. Kuz'mina, and V. S. Rogov, Fiz. plazmy **2**, 858 (1976) [Sov. J. Plasma Phys. **2**, 478 (1976)]; Chislennye metody mekhaniki sploshnoĭ sredy **4**, no. 4, 88 (1973); Teplofiz. Vys. Temp. **6**, 801 (1968); **8**, 689 (1970).
[100]S. A. Maev, Zh. Eksp. Teor. Fiz. **40**, 567 (1970) [Sov. Phys. JETP **13**, 397 (1961)].
[101]D. M. Biberman and G. É. Norman, Usp. Fiz. Nauk **91**, 193 (1967) [Sov. Phys.-Usp. **10**, 52 (1967)].
[102]V. M. Batenin and P. V. Minaev, Teplofiz. Vys. Temp. **15**, 647 (1977).
[103]G. A. Kobzev, Yu. K. Kurilenkov, and G. É. Norman, *ibid.* 193.
[104]Yu. K. Kurilenkov and P. V. Minaev, Zh. Eksp. Teor. Fiz. **74**, 563 (1978) [Sov. Phys. JETP **47**, 295 (1978)].
[105]B. W. Shor, J. Phys. Ser. B **8**, 2023 (1975).
[106]V. S. Lisitsa, Usp. Fiz. Nauk **122**, 449 (1977) [Sov. Phys. Usp. **20**, 603 (1977)].
[107]G. A. Koval'skiĭ and V. G. Sevast'yanenko, Svoĭstva nizkotemperaturnoĭ plazmy i metody ee diagnostiki (Properties of Low-Temperature Plasma and Applicable Diagnostic Methods), Edited by M. F. Zhukov, Nauka, Siberian Division, Novosibirsk, 1977, p. 11.
[108]I. A. Avilova, D. M. Biberman *et al.*, Opticheskie svoĭstva goryachego vozdukha (Optical Properties of Hot Air), Nauka, Moscow (1970).
[109]V. A. Kamen'shchikov, Yu. A. Plastinin *et al.*, Radiatsionnye svoĭstva gazov pri vysokikh temperaturakh (Radiative Properties of Gases at High Temperatures), Mashinostroenie, Moscow (1971).
[110]O. M. Belotserkovskiĭ, L. M. Biberman *et al.*, Teplofiz. Vys. Temp. **7**, 529 (1969).
[111]D. Schlüter, Zs. Phys. **210**, 80 (1968).
[112]G. Bekefi (ed.), Radiation Processes in Plasmas, Wiley, N.Y., (1966) [Russ. Transl., Mir, M. (1971)].
[113]A. F. Nikiforov, V. G. Novikov, N. Yu. Orlov, V. B. Uvarov, Preprint IPM Akad. Nauk SSSR, no. 172, Moscow (1979).
[114]É. I. Asinovskiĭ, A. V. Kirillin, V. L. Nizovskiĭ, and V. I. Shabashov, Teplofiz. Vys. Temp. **8**, 905 (1970).
[115]A. A. Kon'kov, A. P. Rezin, and A. I. Sokolov, *ibid.* **12**, 806 (1974).
[116]B. Yu. Tonkov, Fazovye diagrammy élementov pri vysokom davlenii (Phase Diagrams of the Elements at High Pressure), Nauka, Moscow (1979).
[117]R. Hultgen, P. D. Desai, and O. T. Hawkings, Selected Values of the Thermodynamical Properties of the Elements. Metal Park, 1973. H. K. Mao *et al.*, J. Appl. Phys. **49**, 3276 (1978).
[118]V. E. Fortov, A. N. Dremin, and A. A. Leont'ev, Teplofiz. Vys. Temp. **13**, 1072 (1975).
[119]Ya. B. Zel'dovich, Zh. Eksp. Teor. Fiz. **32**, 1577 (1957) [Sov. Phys. JETP **5**, 1287 (1957)]; Ya. B. Zel'dovich and Yu. P. Raĭzer, *ibid.* **35**, 1402 (1958) [**8**, 980 (1959)].
[120]C. Scidmore and E. Morris, In: Proc. of Symposium on Thermodynamics of Nuclear Materials. I.A.E.A., Vienna, 1962, p. 173.
[121]V. E. Fortov, A. N. Dremin, A. A. Leont'ev, and S. V. Pershin, Zh. Eksp. Teor. Fiz. **20**, 30 (1974) [Sov. Phys. JETP **20**, 13 (1974)].
[122]B. A. Glushak, M. V. Zhernokletov, and V. N. Zubarev, in: Doklady I Vsesoyuznogo simpoziuma po impul'snym davleniyam (Papers at First All-Union Symposium on Pulsed Pressures), Nauka, Moscow, 1974, p. 87.
[123]A. A. Leont'ev, V. E. Fortov, and A. N. Dremin, in: Gorenie i vzryv (Combustion and Explosion), Nauka, Moscow, 1977, p. 575.
[124]L. V. Al'tshuler, A. A. Bakanova, A. V. Bushman, I. P. Dodulanov, and V. N. Zubarev, Zh. Eksp. Teor. Fiz. **73**, 1866 (1977) [Sov. Phys. JETP **46**, 980 (1977)].
[125]L. V. Al'tshuler, A. V. Bushman, M. V. Zhernokletov, V. N. Zubarev, A. A. Leont'ev, and V. E. Fortov, *ibid.* **78**, 741 (1980) [**51**, 373 (1980)].
[126]A. A. Leont'ev and V. E. Fortov, Zh. Prikl. Mekh. Tekh. Fiz. No. 3, 162 (1974).
[127]D. A. Young and B. J. Alder, Phys. Rev. Ser. A **3**, 364 (1971).
[128]K. Horung, J. Appl. Phys., **46**, 2548 (1975).
[129]V. E. Fortov and A. A. Leont'ev, Teplofiz. Vys. Temp. **14**, 1072 (1975).
[130]P. DeBeaumont and L. J. Leygonie, In: Intern. Symposium on Detonation. Pasadena, 1970, p. 430.
[131]K. Hornung and K. W. Michel, J. Chem. Phys. **56**, 2072 (1972).
[132]J. W. Taylor, J. Appl. Phys. **34**, 2727 (1962).
[133]V. E. Fortov, and A. N. Dremin, Fiz. gor. i vzryva **9**, 743 (1973).
[134]S. Drapatz *et al.*, In: XVI Meeting of COSPAR. Konstanza, June 1973, p. 10.
[135]Y. A. Zel'dovich and O. M. Todes, Zh. Eksp. Teor. Fiz. **10**, 1441 (1940).
[136]Yu. A. Alekseev, V. P. Ratnikov, and A. P. Rybakov, Zh. Prikl. Mekh. Tekh. Fiz. No. 2, 101 (1971).
[137]V. E. Fortov, Teplofiz. Vys. Temp. **10**, 86 (1972).
[138]A. V. Bushman, V. E. Fortov, and I. I. Sharipdzhanov, *ibid.* **15**, 1095 (1977).
[139]N. N. Kalitkin, G. V. Kuz'mina, and I. I. Sharipdzhanov, Preprint IPM Akad. Nauk SSSR, no. 43, Moscow (1976).
[140]V. N. Zharkov and V. A. Kalinin, Uravnenie sostoyaniya tverdykh tel pri vysokikh davleniyakh i temperaturakh (The Equation of State of Solids at High Pressures and Temperatures), Nauka, Moscow (1968).
[141]S. B. Kormer, A. I. Funtikov, V. D. Urlin, and A. N. Kolesnikova, Zh. Eksp. Teor. Fiz. **42**, 686 (1962) [Sov. Phys. JETP **15**, 477 (1962)].
[142]S. B. Kormer, V. D. Urlin, and L. T. Popova, Fiz. Tverd. Tela (Leningrad) **3**, 2131 (1961) [Sov. Phys. Solid State **3**,

1547 (1962)].
[143]V. D. Urlin, Zh. Eksp. Teor. Fiz. **49**, 485 (1965) [Sov. Phys. JETP **22**, 341 (1966)].
[144]A. T. Sapozhnikov and A. V. Pershina, collection cited in Ref. 30, p. 101.
[145]C. Boissier and G. Fiorese, Rev. Phys. Appl. **12**, 857 (1977).
[146]E. B. Royse, Rept. UCRL-51121 (1977).
[147]E. Wigner, Trans. Farad. Soc. **34**, 678 (1938).
[148]G. Carmi, J. Math. Phys. **9**, 2120 (1968).
[149]E. L. Pollock and J. P. Hansen, Phys. Rev. **A8**, 3110 (1973).
[150]S. C. Brush, H. L. Sahlin, and E. Teller, J. Chem. Phys. **45**, 2102, (1966).
[151]V. A. Ivanov, I. N. Makarenko *et al.*, Phys. Lett. **A47**, 75 (1974).
[152]N. F. Mott, Phil. Mag. **16**, 49 (1967).
[153]V. A. Alekseev, E. P. Velikhov, and G. A. Lopantseva, in: Electricity from MHD, Vienna, 1966, Vol. 1, p. 214.
[154]I. T. Yakubov and A. A. Khrapak, Usp. Fiz. Nauk **129**, 45 (1979) [Sov. Phys. Usp. **22**, 703 (1979)]; Élektrony v plotnykh gazakh i plazme (Electrons in Dense Gases and Plasma), Nauka, Moscow, 1981.
[155]M. M. Martynyuk, Fiz. gor. i vzryva **13**, 213 (1977); I. Ya. Dikhter and V. A. Zaĭgarnik, Teplofiz. Vys. Temp. **15**, 471 (1977).
[156]W. Chester, in: Problems of Mechanics (eds. H. Draifen and T. von Karman) (Russ. trans.), IL, Moscow (1963).
[157]M. A. Coock, J. Appl. Phys. **26**, 426 (1955); **30**, 1881 (1959); J. Chem. Phys. **24**, 60 (1955); Proc. Roy. Soc. Ser. A **259**, 508 (1961).
[158]M. A. Coock *et al.*, J. Appl. Phys. **29**, 1612 (1958).
[159]G. Ekker and W. Weizel, Ann. Phys. **17**, 126 (1956).
[160]M. A. Coock, The Science of High Explosives. Reinhold, N.Y. (1958).
[161]V. E. Fortov, S. I. Musyankov, V. V. Yakushev, and A. N. Dremin, Teplofiz. Vys. Temp. **12**, 957 (1974).
[162]W. C. Davis and A. W. Campbell, J. Appl. Phys. **31**, 1225 (1960); A. Kendrew and L. Whitbread, In: Symposium on Detonation, ONR, 1960.
[163]E. B. Royce, Phys. Rev. **164**, 929 (1967).
[164]R. G. Arkhipov, Zh. Eksp. Teor. Fiz. **49**, 1601 (1965) [Sov. Phys. JETP **22**, 1095 (1966)]; Fiz. Tverd. Tela (Leningrad) **4**, 1077 (1962) [Sov. Phys. Solid State **4**, 795 (1962)].
[165]L. V. Al'tshuler and A. A. Bakanova, Usp. Fiz. Nauk **96**, 193 (1968) [Sov. Phys. Usp. **11**, 678 (1969)].
[166]D. A. Kirzhnits and G. V. Shpatakovskaya, Zh. Eksp. Teor. Fiz. **62**, 2082 (1972) [Sov. Phys. JETP **35**, 1088 (1972)]; Preprint IPM Akad. Nauk SSSR No. 54, Moscow, 1975.
[167]C. G. M. Van Keesel and R. Sigel, Phys. Rev. **33**, 1020 (1974).
[168]R. E. Kidder, Nucl. Fusion **8**, 3 (1968); C. Fauguignon and F. Flox, Phys. Fluids, **13**, 386 (1970).
[169]R. J. Trainor, H. C. Graboske, K. S. Long, and J. W. Shaner, Reprints UCRL-52562, 80257, 82141.
[170]R. A. Benjamin, G. H. McCall, and A. W. Ehler, Phys. Rev. Lett. **42**, 890 (1979).
[171]L. Vessel and J. Solem, *ibid.* **40**, 1391 (1978).
[172]R. J. Trainor, J. W. Shaner, J. M. Auerbach, and N. C. Holmes, *ibid.* **42**, 1154 (1979).
[173]R. Jachson *et al.*, in: Proc. of VI Intern. Symposium on Detonation. ONR. ACR-221, 1976, p. 775.
[174]D. Steinberg *et al.*, Collection cited in Ref. 6, p. 983. Report UCRL-52752.
[175]N. N. Kalitkin, Zh. Eksp. Teor. Fiz. **38**, 1534 (1960) [Sov. Phys. JETP **11**, 1106 (1960)]; Preprint IPM Akad. Nauk SSSR No. 35, Moscow (1975).
[176]A. K. McMahan and M. Ross, Report UCRL-79050, 1977; in: Proc. of VI Intern. AIRAPT Conference. Colorado, 1978, V. 2, p. 920.
[177]C. E. Ragan III, collection cited in Ref. 6, p. 993.
[178]M. M. Rusakov *et al.*, Teplofiz. Vys. Temp. **13**, 20 (1975); **15**, 449 (1977).
[179]R. Gasner, In: Symposium on High Dynamic Pressure. Paris (1967).
[180]L. P. Volkov, N. P. Vladimirov *et al.*, Pis'ma Zh. Eksp. Teor. Fiz. **31**, 623 (1980) [JETP Lett. **31**, 588 (1980)].
[181]G. V. Sin'ko, In: Chislennye metody mekhaniki sploshnykh sred. (Numerical Methods in Fluid Mechanics), Novosibirsk, VTs SO Akad. Nauk SSSR, Novosibirsk, 1980, Vol. 10, p. 124.
[182]V. A. Alekseev *et al.*, High Temp.-High Pressure **7**, 676 (1975).
[183]H. Renkert, F. Hensel, and E. U. Frank, Ber. Bunsenges. Phys. Chem. **75**, 507 (1971).
[184]W. Freyland, Phys. Rev. **B20**, 5104 (1979).
[185]N. V. Jermokhin *et al.*, J. De Phys. **39**, Nr. 5, Suppl. Cl. (1978).
[186]A. A. Likal'ter, Teplofiz. Vys. Temp. **16**, 1219 (1978).
[187]A. N. Lagar'kov and A. K. Sarychev, *ibid.* **17**, 466 (1978).
[188]A. A. Vedenov, In: Proc. of Intern. Conference on Quiet Plasmas. Frascati, Italy, 1967, p. 107.
[189]M. Baus and L. P. Hansen, Phys. Rept. **59**, No. 1, (1980).
[190]G. E. Duvall and R. A. Graham, Rev. Mod. Phys. **49**, 253 (1977).
[191]L. Davison and R. A. Graham, Physics Rept. **55**, 256 (1979).
[192]O. N. Breusov, in: Detonatsiya. Kriticheskie yavleniya. Fiziko-khimicheskie prevrashcheniya v udarnykh volnakh (Detonation. Critical Phenomena. Physicochemical Transformations in Shock Waves), Chernogolovka, 1978, p. 122.
[193]V. A. Alekseev and A. A. Vedenov, Usp. Fiz. Nauk **102**, 665 (1970) [*sic*].
[194]I. T. Yakubov, in: Fizika plazmy (Plasma Physics), edited by B. M. Smirnov, Atomizdat, Moscow, 1979, No. 1, p. 120.
[195]A. A. Vedenov, in: Voprosy teorii plazmy (Problems of Plasma Theory), edited by M. A. Leontovich, Atomizdat, Moscow, 1963, No. 1, p. 273.
[196]B. M. Smirnov, Vozbuzhdennye atomy i iony v gazakh i plazme (Excited Atoms and Ions in Gases and Plasma), Atomizdat, Moscow, 1974.
[197]S. P. March, Adv. Phys. **24**, 101 (1975).
[198]H. N. Van Horn, Phys. Rev. **157**, 342 (1967).
[199]N. Weiser and M. H. Cohen, J. Phys. **C2**, 193 (1969).
[200]D. Ceperley, Phys. Rev. **B18**, 2126 (1978).
[201]J. T. Devreese, F. Brosens, and L. F. Lemmens, *ibid.* **21**, 1363 (1980).
[202]J. P. Hansen, *ibid.* (1973).
[203]D. A. Kirzhnits, Usp. Fiz. Nauk **119**, 357 (1976) [Sov. Phys. Usp. **19**, 530 (1976)].
[204]O. V. Dolgov and E. G. Maksimov, Usp. Fiz. Nauk **135**, 441 (1981); [Rev. Mod. Phys. **53**, 81 (1981)].
[205]V. A. Sechenov, in: Proc. of XVI C.I.P.I.G., Contributed papers. Minsk, 1981, Vol. 1, p. 357.
[206]R. Radtke and K. Günther, *ibid.* 357.
[207]V. E. Gavrilov and T. V. Gavrilova, *ibid.* 339.
[208]V. V. Vorobiov *et al.*, *ibid.* 361.
[209]W. Bötticher, B. H. Müller, and J.-M. Scheider, *ibid.* 335.
[210]F. H. Ree and M. Ross, collection cited in Ref. 6, p. 927. M. Ross, W. Nellis, and A. C. Mitchell, Lawrence Livermore Lab. Rept. UCRL-82316 (1979).
[211]M. V. Babykin, in: Itogi nauki i tekhniki. Ser. Fizika plazmy (Advances in Science and Technology. Plasma Physics Series), VINITI, Moscow, 1981, Vol. 1, Part 2, p. 5.
[212]B. A. Demidov, A. I. Martynov *et al.*, Zh. Eksp. Teor. Fiz. **80**, 738 (1981) [Sov. Phys. JETP **53**, 374 (1981)].
[213]F. C. Perry and M. M. Widner, Appl. Phys. Lett. **29**, 282 (1976); J. Appl. Phys. **47**, 127 (1976).
[214]M. A. Sweeney, F. C. Perry, and J. R. Assay, Bull. Am. Phys. Soc., **26**, AB9, 650 (1981).
[215]Proc. Impact Fusion Workshop: Los Alamos Rept. LA-I000C (1979).
[216]R. S. Hawke and J. K. Scudder, collection cited in Ref. 6, p. 979.
[217]R. S. Hawke *et al.*, Bull. Am. Phys. Soc. **26**, AB7, 649 (1981).
[218]B. M. Manzon, Usp. Fiz. Nauk **134**, 611 (1981) [Sov. Phys. Usp. **24**, 662 (1981)].
[219]S. I. Anisimov, A. M. Prokhorov, and V. E. Fortov, Lazernaya generatsiya moshchnykh udarnykh voln (Laser Genera-

tion of Strong Shock Waves), RIO OIKhF Acad. Nauk SSSR, Chernogolovka (1981).
[220]V. K. Gryaznov and I. L. Iosilevskiĭ, Teplofiz. Vys. Temp. **19**, 1121 (1981).
[221]C. E. Ragan *et al.*, Bull. Amer. Phys. Soc. **26**, AB5, 649 (1981).
[222]N. C. Holmes, in: Report on High Pressure Research Conference. USA (1980).
[223]Laser Program Annual Report. 1978. Lawrence Livermore Lab. Rept. UCRPL-50021-78, 1979, p. 261.
[224]L. R. Wesser, J. C. Solem, and A. I. Lieber, Appl. Phys. Lett. 35, 761 (1979).
[225]P. D. Goldstone, R. F. Benjamin and R. B. Schaltz, *ibid.* **38**, 223 (1981).
[226]N. H. Benett *et al.*, *ibid.* 226.
[227]R. M. More, Rept. UCRL-50028-79-2 (1979).
[228]B. H. Ripin *et al.*, Phys. Rev. Lett. **43**, 350 (1979); Phys. Fluids, 23, 1012 (1980).
[229]Yu. A. Bondarenko, I. N. Burdonskiĭ *et al.*, Zh. Eksp. Teor. Fiz. **81**, 170 (1981) [Sov. Phys. JETP 54, 85 (1981)].
[230]R. H. Price *et al.*, Bull. Am. Phys. Soc., **26**, AB1, 648 (1981).
[231]N. C. Holmes, R. J. Trainor *et al.*, *ibid.* AB2, 649.
[232]M. A. Sweeney, F. C. Ferry, and J. R. Asay, *ibid.* AB9, 650.
[233]R. Bailly-Salins, collection cited in Ref. 6, p. 986.
[234]S. L. Bogolyubskiĭ, B. P. Gerasimov *et al.*, Pis'ma Zh. Eksp. Teor. Fiz. **24**, 206 (1976) [JETP Lett. **24**, 182 (1976)].
[235]H. Holm, see pp. 205–215 [*sic*]. M. N. Kreisler, *ibid.* 321 [*sic*].
[236]D. E. Tidman and S. A. Goldstein, *ibid.* 285 [*sic*].
[237]S. C. Rashleigh and R. A. Marshall, J. Appl. Phys., **49**, 2540 (1978).
[238]K. E. Froeschner, H. Chau *et al.*, Bull. Am. Phys. Soc. **26**, AB6, 649 (1981).
[239]S. I. Anisimov, V. E. Bespalov *et al.*, Pis'ma Zh. Eksp. Teor. Fiz. **31**, 67 (1980) [JETP Lett. **31**, 61 (1980)].
[240]B. K. Godwal, S. K. Sikka, and R. Chidambaram, Phys. Rev. Lett., **47**, 1144 (1981).

Translated by R. W. Bowers